Cortical Hierarchy and The Dual Counterstream Architecture.

Julien Vezoli[a§], Loïc Magrou[b§], Xiao-Jing Wang[c,d*], Kenneth Knoblauch[b*], Martin Vinck[a*], Henry Kennedy[b,e*]

[a] Ernst Strüngmann Institute (ESI) for Neuroscience in Cooperation with Max Planck Society, 60528 Frankfurt, Germany
[b] Univ Lyon, Université Claude Bernard Lyon 1, Inserm, Stem Cell and Brain Research Institute U1208, 69500 Bron, France.
[c] Center for Neural Science, New York University (NYU), New York, NY 10003, USA.
[d] NYU–East China Normal University Institute
for Brain and Cognitive Science, NYU Shanghai, Shanghai, China.
[e] Institute of Neuroscience, State Key Laboratory of Neuroscience, Chinese Academy of Sciences (CAS) Key Laboratory of Primate Neurobiology, CAS, Shanghai 200031, China

§ equal contributing
* equal contributing, senior authors

Abstract
Hierarchy is one of the major organizational principals of the cortex and underscores modern computational theories of cortical function. Based on a review of the literature on the local microcircuit and its role in the amplification of inputs, we develop the argument that distance dependent changes in connectivity and oscillatory coherency of the inputs to an area represent the structural and functional signatures of hierarchy. Statistical modeling of these structural signatures demonstrates that inputs from multiple levels to target areas across different levels show remarkable consistency. Close examination of inter-areal connectivity reveals a dual counterstream architecture with well-defined distance-dependent feedback and feedforward pathways in the supra- and infragranular layers, suggesting a multiplicity of feedback pathways with well defined functional properties. These findings are coherent with feedback connections providing a generative network involved in a wide range of cognitive functions. Exploring the laminar basis of inter-areal interactions, we suggest, can be overcome with concerted experiments capitalizing on recent technical advances in tract-tracing, high-resolution fMRI and optogenetics thereby allowing a much improved understanding of the computational properties of the cortex.

Keywords
Non-human primate, mouse, electrophysiology, anatomy, modeling

Plan

1. Introduction
2. Hierarchy – signatures of inputs to the local circuits.
3. Hierarchy – input consistency
4. Dual stream architecture.
5. Functional characteristics of FF and FB pathways.
6. Diversity of pathways and their function in neural computations
7. Top down generative networks
8. Conclusion.

1. Introduction

Hierarchy as an organizational feature of the brain has been a recurrent theme since the evolutionary theory of neurological disorders of the neurologist John Hughlings Jackson (1835-1911), following his observations of positive and negative symptoms in his patients (York and Steinberg, 2011). The neurobiology of cortical hierarchy was explored by the pioneering work of David Hubel and Tornsten Weisel who characterized the receptive field properties of simple, complex and hypercomplex neurons across areas of the visual cortex (Hubel and Wiesel, 1962). Very quickly a myriad of connectivity studies in the cortex found additional evidence of hierarchical organization, allowing Felleman and Van Essen to propose the first hierarchical model of the cortex (Felleman and Van Essen, 1991), thereby providing a framework for modern concepts of feedforward and feedback processes. The notion of hierarchy has become considerably generalized and for example can be considered to be the major concept linking biological and artificial intelligence (Hawkins and Blakeslee, 2004). For example, convolutional deep neural networks have a clear hierarchical organization, with convergent, feedforward connections passing information from lower to higher layers, and divergent feedback connections shaping plasticity in the connections from lower layers. But what exactly is the significance of hierarchy in the brain? Hierarchy has been extensively studied in terms of ranking of cortical areas with respect to a number of criteria including, gradients of structural and functional features, as a progression of scales or as a topological sequence of projections (Hilgetag and Goulas, 2020). Here we take a diametrically opposing view. In line with the tenet that the explanation of how the brain works demands an account of what neurons do, and that functional interactions of cortical areas is assured by neuronal activity relayed between areas by axons, we confine our discussion of hierarchy to the description of the neuronal properties of inter-areal relations. We propose that the structural and functional markers of hierarchy laminar projection patterns define the integration of long-range inputs into each local circuit. These signatures represent structural and functional regularities, which we argue provide important insight into understanding the input requirements of cortical areas and, therefore, clues to the cellular mechanisms underlying the mode of operation of individual areas. A critical aspect of these regularities concerns the spatial distances governing interactions between cortical neurons, which we and others have shown establish metabolic constraints on the cortex and which underlines the spatial embedding of the cortex (Markov et al., 2013).

2. Hierarchy – signatures of inputs to local circuits.

In 1989 Douglas, Martin and Whitteridge published a landmark study in cat cortex that proposed a canonical microcircuit for the neocortex (Douglas et al., 1989) (Figure 1 and 12b). A common misconception of the canonical microcircuit is that it originates uniquely from a consideration of the inter-laminar wiring patterns of the cortex. In fact it is much more a theory that attempts to explain the electrophysiological properties of the cortex in terms of local connectivity including inter-laminar connections. In an effort to nail down the transformation of the thalamic input, *in vivo,* intracellular recordings in anesthetized cats by these authors showed that minute inputs from the LGN are amplified by recurrent excitation in layer 4 neurons of area V1. Later, quantification of the synaptic components of the local circuit by the group of Martin and Douglas showed that recurrent excitation was a characteristic feature of the local circuit (Figure 1) (Binzegger et al., 2009). Further, contrary to what was previously thought, the role of inhibition was not to carve out the selectivity of the neuron response but rather to exert a control over the amplitude of the response. In this way they found that inhibitory potentials were maximized in the optimal receptive field response (Douglas et al., 1995; Douglas et al., 1989). Initially these researchers thought that, contrary to what had been proposed by Hubel and Wiesel, the geometry of the thalamic input into the cortex was not the primary cause of orientation selectivity. David Ferster later showed that there is a weak

orientation response in the input to the cortex, meaning that the primary role of the recurrent excitation is the amplification of a signal and not its creation (Ferster et al., 1996).

Here Figure 1

For many years research on cortex was predominantly in carnivores and non-human primates, leading to the notion of the cortical column as an explanation of functional organization (Mountcastle, 1995). In these studies, electrophysiological recordings from electrode penetrations made perpendicular to the cortex found a conserved function in the width of the cortex in passing from pia to white matter (Hubel and Wiesel, 1962; Mountcastle, 1957). In the visual system there were expectations that the columnar organization of the cortex would be both functional and structural, since physiologically demonstrated ocular-dominance columns seemed to co-localize with cortical territories labeled by transynaptic labeling following tracer injections in the eye (Hubel and Wiesel, 1977). However, close examination revealed important discrepancies in such a correspondence (reviewed (da Costa and Martin, 2010)), suggesting that the link between cortical structure and function is to be found at a much finer scale. Thanks to work in the mouse visual cortex using the molecular tools that are available in this species, it has been confirmed that cortical responses to thalamic input are indeed the consequence of an amplification (Harris and Mrsic-Flogel, 2013) (Lien and Scanziani, 2013) via the local recurrent excitation (Cossell et al., 2015; Douglas et al., 1995; Ko et al., 2011). These studies built on earlier findings of highly nonrandom features of synaptic connectivity in local cortical circuits, proposing that there is a skeleton of strong connections in a sea of weak connections (Song et al., 2005). Later it was shown that the rare strong connections in the lognormal distribution of synaptic weights are between neurons with similar receptive fields, meaning that neurons in the visual cortex listen most closely to a subset of their synaptic inputs (Cossell et al., 2015). These findings are most satisfying as they explain earlier observations showing that ongoing activity of a neuron (so called spontaneous activity) reflects the functional architecture (i.e. the backbone of strong connections) in which it is embedded (Tsodyks et al., 1999). The emerging picture is that layers 4, 3 and 2 neurons are organized into subnetworks so that the selectivity of the amplification is ensured by restraints at the scale of dendritic spines (Lee et al., 2016). Finally, while the notion of selective amplification of a small input is maintained, refined neuroanatomical techniques suggest that the thalamic input in terms of proportions of synapses is near 20%, considerably higher than previously thought (Garcia-Marin et al., 2019).

The principal wiring property of the canonical circuit is the recurrent excitation that is observed in all of the cortical layers including layer 4 (Binzegger et al., 2004). The relevance of the canonical microcircuit theory for understanding inter-areal processing became apparent when cortical connectivity was quantified. It turns out that 80-90% of the connections of the cortex are in the local circuit spanning 1-2mm in the visual cortex (Markov et al., 2011). Except for the adjacent cortical area, the structural weight of the average input from a distant source area to a target area is several orders of magnitude *less* than the thalamic input (Markov et al., 2014a). These observations lead to the notion that amplification by local recurrent excitation is a general phenomenon, but that it should differentially impact inputs to the cortex (Douglas and Martin, 2007a, b). For instance, top-down signaling of selection attention multiplicatively modulates sensory neurons by a small amount (McAdams and Maunsell, 1999; Treue and Maunsell, 1996), which is amplified by local circuit dynamics leading to all-or-none task switching (Ardid and Wang, 2013).

Early anatomists, working principally in non-human primates, distinguished between rostral directed connections that originate chiefly in the supragranular layers and terminate in layer 4 (Cragg, 1969; Kennedy and Bullier, 1985; Lund et al., 1975; Martinez-Millan and

Hollander, 1975; Rockland and Pandya, 1979; Spatz et al., 1970; Van Essen and Zeki, 1978; Wong-Riley, 1978) and caudal directed connections that mostly originate from infragranular layers and terminate outside of layer 4 (Kaas and Lin, 1977; Kennedy and Bullier, 1985; Kuypers et al., 1965; Tigges et al., 1973; Wong-Riley, 1978). In a landmark study, Rockland and Pandya (Rockland and Pandya, 1979) were the first to formulate inter-areal connectivity in terms of hierarchy and suggested that the laminar organization of cortical afferents and their terminals indicates the sequence of information processing in cortex. These authors proposed that connections originating from supragranular layers and terminating in layer 4 by analogy with the main thalamic input to cortex constitute the feedforward pathway channeling sensory information to cortical areas carrying out higher order analyses. By contrast connections arising from the infragranular layers, by analogy with descending projections to subcortical structures, correspond to feedback connections that enable higher order areas were postulated to modulate the activity of lower level areas (Rockland and Pandya, 1979).

The classification of pathways between areas as feedforward and feedback helped motivate the role of the cortical network in terms of feedforward pathways shaping receptive fields in their target areas (Hubel, 1995) and feedback pathways relaying contextual information (Gilbert and Li, 2013; Zipser et al., 1996). How the inter-areal network related to the mosaic of cortical areas was given substance by Fellleman and Van Essen's pairwise-comparison of pathways between areas showing that the layout of cortical areas corresponded to a distributed hierarchy (Felleman and Van Essen, 1991), that agreed with a distance rule (Kennedy and Bullier, 1985). The quantification of the laminar distribution of retrograde labeled neurons following injection in a target area shows that there is a gradient of decreasing labeled supragranular neurons going from high to lower hierarchical levels and an increase going from low to higher hierarchical levels (Barone et al., 2000; Kennedy and Bullier, 1985; Markov et al., 2014b). These findings can be summarized as a hierarchical distance rule, and reflect a smooth gradient of inputs of neurons in different layers and areas to a target area (Figure 2).

Here Figure 2

One way of thinking about connectivity gradients (Figure 2a) is that they represent gradual changes in the composition of inputs to the local microcircuit of a cortical area that is distance-dependent. If these changing inputs to the local microcircuit represent the structural signature of hierarchy it is legitimate to wonder if they have a functional correlate. When frequency-specific directed influences of rhythmic synchronization are correlated with hierarchical distance it shows that feedforward pathways are characterized by synchronization in the theta (4 Hz) and gamma-band (60-80 Hz) and feedback in the beta-band (14-18 Hz) (Bastos et al., 2015b). These findings suggest that the structural signatures to the microcircuit are indeed paralleled by functional signatures. However, whereas the structural hierarchy is fixed the functional hierarchy exhibits task dependent dynamics. Here we set out to formalize the way that inputs to a given area are shaped by distance.

3. Hierarchy – Input Consistency.

The notion of hierarchy implies order or rank, so that determining if there are hierarchical relations between cortical areas reduces fundamentally to determining if order relations can be defined between them. For example, the Felleman and Van Essen hierarchy (FVH) was based on the notion of feedback/feedforward relations between areas defined by laminar origin and termination of projections (Felleman and Van Essen, 1991) that originated in earlier observations of laminar patterns of connectivity. A feedforward connection was defined as originating in supragranular layers and targeting layer 4. A feedback connection was defined as originating in infragranular layers and avoiding layer 4. A feedforward

projection from area A to B implied that B was ordered after A. Similarly, a feedback projection from B to A would also be consistent with the above feedforward relation in assigning B after A. Note that in the above description there are two criteria for ordering the areas, whether they are in a feedback or whether they are in a feedforward relation. The two criteria do not have to agree. On a simple level, disagreement could be taken to define equality of ordinal levels in the sense that equality is defined as those numbers, A and B, that simultaneously satisfy $A \geq B$ and $A \leq B$. Alternatively, distinct hierarchical orders might arise: one on the basis of feedforward laminar projections, the other on the basis of feedback. This is a point that might become important when the data supporting multiple laminar feedback/feedforward pathways are analyzed.

A notable aspect of the criteria for determining hierarchical rank described above is that they are based on properties of projections, or more generally relations, between areas. As an alternative, one might consider properties that are intrinsic to an area, such as cortical thickness, neuron density, soma size, spine count, spine density and dendritic tree size. These properties have been shown to display a smooth variation across the cortex that allows ranking of areas in accordance with the gradation principle of Sanides (Barbas, 2015; Sanides, 1972). Because these properties vary across the cortex, then a hierarchical ranking can be established trivially by ordering the areas according to the property. This distinction leads us to consider that criteria for building cortical hierarchies can be divided into two broad classes that we shall refer to as *node-based* and *link-based* (Figure 3).

Here Figure 3

The Felleman and Van Essen hierarchy is a link-based criterion because it depends on the projections between areas. Other examples of link-based criteria that could be used as measures of inter-areal organization include the Fraction of Labelled Neurons (FLN) projecting to an area (Markov et al., 2014a; Markov et al., 2011) and Granger causality (Bastos et al., 2015b; Michalareas et al., 2016). Earlier work (Barone et al., 2000; Markov et al., 2014b; Vezoli et al., 2004), has used a quantitative estimation of hierarchical distance, based on the proportion of projections originating in supra-granular layers with respect to all of the projections originating from the area and that we refer to as the proportion of Supragranular Labelled Neurons (SLN) and that has led to the Hierarchical Distance Model (see Figure 2).

Here it is useful to draw an analogy with social networks. A hierarchy in a social network implies that the actors show specific kinds of interactions with each other (*link-based*). Hierarchy implies that those close to each other in a hierarchy show stronger interactions with each other than actors that are distant in the hierarchy. More information can be gauged from the nature of the interactions: We expect that someone high in the hierarchy (a boss) will show a more directive communication pattern to workers lower in the hierarchy. The workers, in turn, will show a different ascending communication pattern, e.g. asking more questions. Thus, a hierarchy can be constructed by studying the way in which people interact with each other, and knowing a hierarchy could in principal allow us to predict these interactions. By analogy, the SLN can be seen as a measure that directly quantifies the nature of the interactions between brain areas, based on the laminar projection patterns. Interestingly, these laminar projection patterns also relate to certain functional interaction patterns (feedforward gamma and feedback alpha/beta influences). In addition, social hierarchy might also be gauged from properties of the people in the hierarchy themselves. For instance, one expects the boss of the company to have the largest office, but the workers at the bottom to share an office and have smaller desks (*node-based*). In some sense, one could argue however, that the *node-based* view is based only on indirect markers and is ultimately grounded in the interaction link-based view.

There are critically important differences for constructing hierarchies between node and link based information. By definition, node-based relations depend only on a value intrinsic to the node, not the relations between nodes so they give no information on the symmetry or otherwise of inter-areal relations, in other words ranks based on connectivity patterns are expected to show reciprocity, so that if there is FF pattern from area A to area B, a feedback pattern is expected from area B to area A. Node based criteria are always defined between any two areas independently of whether or not a connection is actually present. Link-based criteria can provide information on asymmetric relations, provided they are directional and are strictly defined between areas only when there is a direct connection. Nevertheless, hierarchical ordering between unconnected areas can be achieved through indirect connections. Generally, links describe the connections that are carrying information between areas and therefore the manner in which the connections and activity are integrated into the local circuit of the target area and source areas.

Here Figure 4

In order to define a hierarchical distance scale, i.e., that is not just ordinal, a distance function, d must be defined. This function d should transform whatever anatomical or physiological measure one is using into a consistent measure of hierarchical distance across cortical areas. For example, Figure 4 shows a hypothetical distance scale on which 4 areas, A, B, C, D, are arranged. Suppose that hierarchical distances can be estimated based on measures derived from tracer injections in areas A and B. The injection in area A provides information about hierarchical distances to areas B, C and D and the injection in B to areas A, C and D. A consistent measure of hierarchical distance, d, would generate the same estimate of distance, d_{AB}, between areas A and B or, formally, we would expect that $d_{\mathrm{CA}} - d_{CB} = d_{\mathrm{DA}} - d_{DB}$. This is easily derived from the two equations in Figure 4 that show for two areas, C and D, the expected relation between the hierarchical distances of a common area to C or D to two injection sites, A and B. For common projections X, plotting d_{XA} against d_{XB} should fall along a line of unit slope with intercept d_{AB}. The question is how to define the distance function d.

Felleman and Van Essen derived an ordinal hierarchy of visual areas based on a binary measure of connectivity, indicating whether the laminar connectivity pattern indicated that an area was in a feedback or feedforward relation with another area. The derived hierarchy was criticized as being indeterminate (Hilgetag et al., 1996) because the data permitted 150,000 equally plausible orderings other than the one proposed by Felleman and Van Essen. Barone et al. (2000) (Barone et al., 2000) resolved this issue by quantifying the laminar relations via SLN, defined above. SLN is a continuous measure on the interval (0, 1), thus providing a measure of the degree of feedforwardness/feedbackness. A binary description treats a projection as feedforward (feedback) if its SLN is greater (less) than 0.5. Using simply the SLN differences as a hierarchical distance measure, they were able to reproduce nearly all of the features of the FVH based on the SLN values from injections in just two areas, V1 and V4. A notable exception from the FVH is that the frontal eye field (FEF) was placed below the early visual area V4. SLN values from FEF to V4 was above 0.7 which placed V4 at higher hierarchical levels. Subsequent physiological studies confirmed FEF role in early visual processing (Moore and Armstrong, 2003; Schall, 2015) thus validating its relatively low hierarchical level. The unusual feedforward pattern for such a caudally directed projection was further confirmed in other studies (Pouget et al., 2009) and pertains to a specific link-category on which we expand later.

Here Figure 5

While differences in SLN establish a determinate hierarchical distance measure between areas, the measure is not necessarily consistent in the manner described in Figure 4. As the measure is defined on the interval (0, 1), SLN differences for the two areas projecting to a third area are expected to be quite different from those to another more distant area. An ideal, measure would project the interval (0, 1) to a scale where differences are always linear. This is commonly accomplished in statistical models, such as generalized linear models (GLM), with a logit or probit transformation (Figure 5) that map the unit interval onto the real line. As the figure demonstrates, with the proper scaling both of these transformations yield rather similar mappings.

Figure 6 shows a set of scatter plots for SLN values of common projections for all area pairs between each of 11 visual areas injected with retrograde tracer (Markov et al., 2014b). The SLN values are plotted on probit transformed axes. For many of the area pairs, the point distributions are reasonably well described by a line of unit slope (dashed blue in each graph), as predicted by a consistent measure of distance, i.e., $SLN_j = SLN_i + c$, where c is a constant. Given the similarity of the transforms, it is not surprising that the logit transformation yields virtually the same linear patterns between area pairs. Thus, this indicates that the ratio of supra- and infra-granular projections follows a gradient across the cortical areas and constitutes a global signature of hierarchical distance among these areas.

Here Figure 6

Is this laminar pattern of connectivity specific to the visual system or is it a more general principle of organization of feedback and feedforward pathways in the brain? In support of the latter hypothesis, Figure 7 shows paired scatter plots of SLN values for a set of 8 somatosensory and motor areas in the same format as Figure 6. As in the visual system, the probit transformed SLN values provide evidence of a consistent distance measure in the hierarchical organization among these areas.

Here Figure 7

Based on this consistency we proposed a model to estimate hierarchical distances based on SLN values. In short, we suppose that we can assign a hierarchical level, h_i and h_j, to all areas i and j,

$$g\left(\mathrm{SLN}_i^p\right) - g\left(\mathrm{SLN}_j^p\right) = h_i - h_j,$$

where g is a transformation of SLN values, such as the logit or probit transform described above, from an injection into area p that receives projections from areas i and j. This suggests a formalism similar to a GLM with a binomial family. The SLN is taken as a binomial variable (neurons are found in the upper or lower cortical layers) and the sum of neurons in both compartments is used as a weight. The hierarchical relation between the weights is a linear predictor that determines a model matrix that is given by the incidence matrix for the graph, $\boldsymbol{X}$, of connections between areas.

$$g\left(\mathrm{SLN}_i^p\right) = \boldsymbol{Xh}$$

where $\boldsymbol{X}$ has a row for each projection and a column for each area. For a given projection there is a -1 in the target area and a 1 in the source, all other column entries being 0. The vector h contains the hierarchical coefficients to estimate and its length is equal to the number of columns of the model matrix. The model as defined is not identifiable because the sum of every row equals 0, but by dropping one column, for example, area V1 in the visual hierarchy, the hierarchical coefficients can be estimated with the area corresponding to the dropped row fixed at a hierarchical level of 0.

This resembles a logistic or probit regression problem. However, these models yield standard errors for the estimated coefficients that are unrealistically small. Alternatively, we have used a beta-binomial model, this arises naturally as a binomial model in which the parameter p, indicating in the current context the expected SLN value, has variability greater than that specified by the binomial distribution and its distribution is described by a beta distribution (Lesnoff and Lancelot, 2012). For the purposes here, the model can be reparameterized to include a dispersion parameter that better models the overdispersion typically observed in neural counts (see (Markov et al., 2014a) for further details). Once the statistical model is specified, the coefficients are estimated by maximum likelihood. The formalization is quite general. For example, if instead of SLN, a binary variable is used simply specifying whether a connection is of a feedforward or feedback type, then the model corresponds to the original problem that Felleman and Van Essen solved. We have found that fitting the model in this fashion leads to coefficients with very large standard errors, in accord with the analyses indicating the indeterminacy of their solution. Thus, the use of a quantitative measure of hierarchy leads to a more exact solution.

Here Figure 8

The visual hierarchy estimated from our model is shown in Figure 8 (left) panel and resembles qualitatively the FVH. In contrast, the levels are continuously distributed. Here we have split FEF into two areas, 8L and 8M corresponding to regions involved in small and large saccades, respectively. Area 8L occupies a low position in the hierarchy while 8M is several levels higher. The goodness of fit of the model is indicated by plotting the empirical SLN values against those predicted by the model (right panel) and shows that the model accounts for a high proportion of the variance in the data. The functional implications of this model have been explored in several contexts (Bastos et al., 2015b; Chaudhuri et al., 2015; Magrou et al., 2018) and preliminary observations indicate that it is applicable to data from the mouse (D'Souza et al., 2020).

The use of a transformation of SLN to estimate hierarchical distance imposes strong constraints on inter-areal SLN relations. We demonstrate this in Figure 9 by using the logit transform, which performs quantitatively nearly identically to the probit transform (Figure 5), but allows expression of the hierarchical relations in terms of ratios of projection strengths. The model defines hierarchical distance, h_{ij}, between two areas, i and j, as the difference between the logit of SLN values for their projections to a target area, p, shown in the top equation. For the logit, this distance is just the natural log of the ratio of ratios of supra- to infragranular projection strengths from areas i and j to p (orange arrows in Figure 9a). If the hierarchical distance measure is consistent, we expect that ratio to be the same for projections to any other area, q, (blue arrows in Figure 9a) as shown by the equation below the diagram. A simple rearrangement of this identity demonstrates that the ratio of projections from area i to areas p and q (orange arrows in Figure 9b) should be the same for any other area j, projecting to areas p and q. Thus, the hierarchical model we propose implies strong invariances in the ratio of feedforward to feedback projection strengths from common inputs and outputs across areas. We further hypothesize that these invariances impose constraints on the exchange and stability of information flow across the cortical hierarchy.

Here Figure 9.

One might suppose that when dual retrograde tracer injections are made in reciprocally connected areas that the pair of areas would display a reciprocal feedforward-feedback relation. That is to say, the origin of the majority of projections from one area would arise from upper

layers and the principal origin of the reciprocating projections from lower layers. This arrangement would naturally lead to the hierarchical regularities that we observe. However, this regularity is not imposed by our model, and it is not always found to occur. In effect, this is what explains the surprising observation (noted above in the hierarchy derived in Figure 8) of a prefrontal area like 8L at the same hierarchical level as early visual areas V3 and V4. As expected, the projections from several lower order visual areas, e.g., V4 and TEO, to area 8L originate in upper layers signifying feedforward, projections. However, 8L projects back to these areas through feedforward projections also originating in upper layers (Barone et al., 2000; Markov et al., 2014b). We designate such feedforward-feedforward connections as strong loops (Crick and Koch, 1998). They correspond to the situation described earlier in an order relation that when $A \geq B$ and $B \geq A$, then $A = B$.

Here Figure 10.

In the FVH model, feedforward (feedback) projections connect upstream (downstream) areas in a bottom-up (top-down) fashion placing hippocampus, anterior temporal and prefrontal areas at the top and occipital areas at the bottom of the visual hierarchy. As such, this model described two main counterstreams involved in hierarchical processing within the visual system: a rostro-caudal gradient of feedback (FB) projections reciprocated by a caudo-rostral gradient of feedforward (FF) projections. Interestingly, in the data base of visual areas on which the FVH was based, only one pathway have been reported – between FEF and CITd (dorsal part of inferior temporal cortex) that corresponds to a strong loops. This led Crick and Koch (Crick and Koch, 1998) to speculate that such configurations were forbidden in cortical organization. On the contrary, we have identified a significant number of them in our data base. Figure 10 shows how the $\log_{10}$ FLN varies as a function of distance estimated through the white matter from the source area to the target injection site, referred to as white matter (WM) distance), replotted from Ercsey-Ravasz et al. (Ercsey-Ravasz et al., 2013). The beige points correspond to those connections that participate in strong-loops i.e. area pairs for which SLN is greater than 0.5 in both directions. For reference, the saturation of these points indicates their SLN values with less saturated points indicating a higher SLN, as shown by the inset color bar. As expected, most of the SLN values near 1 cluster to the right as more long distance connections. There is a fair amount of scatter among the points but they do display a distance rule (blue regression line) just as the rest of the connections do (black regression line). Interestingly, when WM distance is accounted for the strength of the strong loop projections is on average greater than the rest of the projections. This suggests that they are likely to play a unique role in cortical computation. What that role is currently remains a mystery. However, some experimental evidence are in favor of an attentional role concerning the strong-loop between FEF and V4. FEF projections can drive attentional response in V4 (Moore and Armstrong, 2003), through selective gating of V4 receptive-fields (Armstrong et al., 2006). Further evidence points to the involvement of fast rhythmic synchronization during FEF attentional modulation of V4 visual responses (Gregoriou et al., 2012; Gregoriou et al., 2009), strongly suggesting a supragranular origin (Bastos et al., 2015a; Markov et al., 2014b).

The results reveal a high-degree of consistency of the structural regularities underlying cortical hierarchy in the sensory cortex. But how generalizable are these findings across the more anterior regions, particularly in frontal and prefrontal cortex (Badre and D'Esposito, 2009; Choi et al., 2018)? One of the few studies that has addressed the structural hierarchy with tract tracing of the prefrontal cortex (Goulas et al., 2014) found little evidence of the rich rostral to caudal hierarchical organization that has been reported in human imaging studies (Badre and D'Esposito, 2007; Koechlin et al., 2003). The controversial issue of frontal cortex and hierarchical control shows promise of resolution via a revision of the concept of a unitary model

ensuring a unidimensional gradient. Recent reports favor distinct networks which it is proposed interact to ensure a global hierarchical structure (Schumacher et al., 2019). Nevertheless, the mismatch between the multistage cascade architecture mediating a temporal organization of cognitive control and inter-areal connectivity contrasts with the situation in the visual cortex where there is a smooth increase in receptive field size ascending the Felleman and Van Essen cortical hierarchy (Roelfsema and de Lange, 2016). The mismatch reported in the prefrontal cortex is between the concept of a smooth and gradual rostral-caudal organization found in the imaging studies and the connectivity as found in the collated and binary data base. What about the relation of SLN across prefrontal areas? In Figure 11 (left), the SLN pairs plots for the prefrontal cortex show an encouraging agreement with that described in visual cortex. The hierarchical scale values estimated from the statistical model described above (Figure 11, right) seem to support a rostral-caudal organization with F1 at the bottom and areas 10 and 24c (the most anterior limbic region) at the top. Note, analysis based on more complete coverage of the frontal cortex might give significantly improved results.

Here Figure 11

4. Dual stream Architecture.

In the preceding section we showed that the contributions of supra- and infragranular layers in the projections across hierarchical levels were highly consistent. Here we explore the hypothesis that FB signals in upper and lower layers have distinct roles in information processing. There are a number of reasons for thinking that this might be the case. In corticogenesis the supragranular compartment is generated by a primate-specific germinal zone (Smart et al., 2002), exhibiting uniquely complex lineages (Betizeau et al., 2013; Dehay et al., 2015; Lukaszewicz et al., 2005), findings that have consequently been amply confirmed in human corticogenesis(Geschwind and Rakic, 2013). These specialized developmental origins of the supragranular layers are linked to the observed expansion of these layers in primates (Cahalane et al., 2014), and a diversification of cell-types, which we speculate underlies the observed coding properties of these layers in the adult primate cortex (Tang et al., 2018; Vinje and Gallant, 2000; Wang and Kennedy, 2016; Willmore et al., 2011). A number of studies have shown that supragranular layers exhibit sparse coding in which large numbers of cells are characterized by low levels of activity and a sensory stimulus activates only few neurons (Barth and Poulet, 2012; Crochet et al., 2011; Haider et al., 2013; Harris and Mrsic-Flogel, 2013; Petersen and Crochet, 2013; Tang et al., 2018). Hence, in a sparse code information is encoded at any instant by the spiking of a small number of neurons, as opposed to a dense code where overall activity is high and information is encoded by variation in firing rate as observed in the infragranular layers (Sakata and Harris, 2009). A sparse code reduces redundancy and is arguably more efficient. Studies indicating sparse coding in supragranular layers find evidence of higher levels of recruitment of inhibitory drive in these layers via fast spiking PV+ neurons (Hu et al., 2014), which supports the presence of distinct frequency channels for FB and FF communication (Bastos et al., 2018; Bastos et al., 2015b; Michalareas et al., 2016). In addition, sparse coding, supragranular neurons in V1 showed more complex and specific selectivity than expected for primary visual cortex (Bonnefond et al., 2017).

Here Figure 12

A more detailed description of the laminar organization of inter-areal connectivity suggests that variation of SLN with distance has complex origins concerning inter-areal connectivity in sublayers of the cortex. Exhaustive examination of inter-areal connectivity

shows, that whereas canonical FB streams have been traditionally allocated to infragranular layers, a robust supragranular FB stream is in addition found in layer 2 (L2) in all areas examined in the extrastriate visual cortex of the macaque (Figure 12a) (Markov et al., 2014b). In addition to the L2 FB, we found some evidence of a L5 FF stream. Hence, in both upper *and* lower compartments there is a counter stream leading to the term dual counterstream architecture. The strict segregation of FF and FB streams was hypothesized by Ullman in his counterstream model, which he proposed allows a bi-directional search for optimal matches between descending and ascending pathways (Ullman, 1995, 2000).

Closer examination of the individual streams showed that each obeys a unique hierarchical distance rule. In all streams labeled cell counts decline with WM distance, however the rate of decline is characteristic for a given stream. In this way, the classical FB stream in L6 of the infragranular layers has the most gradual decline so that these FB connections span the biggest distance in the cortex. This contrasts with the L2 FB, which shows a much shorter space constant. Hence it is the combination of the space constants of the L2 and L6 FB streams that leads to the observed SLN values going up stream from near to far-distant areas (See Figure 13). The classical FF stream in L3 is also long-distance stream, but significantly less than the FB L6 stream, thus leading to the observation of the greater reach of FB pathways compared to FF pathways.

Here Figure 13

Hence, the dual counterstream architecture shows that the relative rate of decline in individual streams determines the way that SLN is modulated by WM distance. In section 3 (Hierarchy –input consistency) we showed that the agreement between SLN values across hierarchical levels is relatively constant across the extrastriate macaque cortex, but less so for the prefrontal cortex. These differences between frontal and posterior regions could be driven by two sets of factors. Firstly, quite simply the space constant can change in individual layers so that the two regions sample supra- and infragranular layers over different WM distances. For example, if the difference in space constants of L2 and L6 FB streams are reduced then so are the SLN differences and there will be a reduction of the hierarchical distance as such between a group of areas with a common target. A second factor could be the identity of cells in the two streams. Comparison of the gene expression across species has revealed that some genes in rodents that are exclusively expressed in deep layers are expressed in the supragranular layers of primates (Zeng et al., 2012). Such changes in the laminar phenotype could perhaps occur across regions meaning that the L2 FB pathway in the prefrontal cortex may not correspond to the same identities as the FB pathway in extrastriate cortex.

5. Functional characteristics of FF and FB pathways.

In the present review we propose that cortical hierarchy can be gauged from the *nature* of the interactions between different brain areas, in the same manner that hierarchies in social networks reflect the nature of interactions between people. Crucially, our measure of hierarchical distance shows that SLN values of area pairs are highly consistent across multiple hierarchical levels. This consistency in conjunction with the known differences in oscillatory properties of laminar compartments of the cortex suggests that FF and FB interactions are not only anatomically distinct, but (i) use specific frequencies for communication and (ii) play specialized roles in cortical computation. Here we address how these functional properties relate to the detailed anatomical properties of FF and FB pathways.

We and others have shown that the *functional nature* of interactions between brain areas like structural hierarchy also depends on hierarchical distances (Bastos et al., 2015b; Michalareas et al., 2016; Richter et al., 2018; van Kerkoerle et al., 2014). Granger-causality

was used to quantify functional FF and FB interactions, thereby allowing the strength of these interactions to be quantified for individual frequency bands. Neuronal populations show spontaneous fluctuations over time that are driven by brain rhythms in different frequency bands, such as theta (3-8Hz), alpha (8-12Hz), beta (12-30Hz) and gamma (30-80Hz). Note, neocortical rhythms do not comprise band-limited sinusoidal oscillation but typically describes noisy oscillations with energy in a wide frequency range (Burns et al., 2011; Spyropoulos et al., 2019). FF Granger-causality is particularly strong in the gamma-frequency band, while FB Granger is strong in the alpha and beta-frequency band (Bastos et al., 2015b; Michalareas et al., 2016; Richter et al., 2018; van Kerkoerle et al., 2014).

The finding that Granger-causality in the FF (FB) direction is strong in gamma (alpha/beta) frequencies is partially dictated by the cellular targets of inter-areal pathways. FF inputs target both excitatory and GABAergic interneurons (Figure 14). Importantly, the FF projections to GABAergic interneurons target almost uniquely parvalbumin – PV interneurons, which are associated with gamma-frequency rhythms and respond to excitatory inputs with high temporal fidelity (Buzsaki and Wang, 2012; Cardin et al., 2009; Jouhanneau et al., 2018; Wang, 2010), and exhibit supra-threshold resonance at gamma-frequencies (Hasenstaub et al., 2005; Pike et al., 2000). Moreover FF projections skip the infragranular layers that are canonically associated with alpha and beta rhythms (Bollimunta et al., 2008; Buffalo et al., 2011; van Kerkoerle et al., 2014). By contrast, FB projections target multiple classes of GABAergic interneurons. Of these, somatostatin – SSt interneurons are associated with the generation of slower brain rhythms (Moore et al., 2010), and can directly influence activity of neurons in infragranular compartments, which are associated with alpha/beta rhythms.

Here Figure 14

Frequency-specific information transmission can also be predicted by the properties of the *sending* and *receiving* areas, so that the global distribution of brain rhythms across areas and layers contribute to the nature of functional interactions in the FF and FB directions. Gamma-rhythms are particularly strong in early visual areas *and* superficial layers (Bastos et al., 2015a; Buffalo et al., 2011; van Kerkoerle et al., 2014; Vinck and Bosman, 2016), whereas beta rhythms are most prominent in fronto-parietal areas *and* infragranular compartments (Bastos et al., 2015a; Buffalo et al., 2011). Consequently, one expects Granger-causal FF influences from early visual areas to parietal areas to be dominated by gamma frequencies, whereas FB influences to visual areas to be dominated by beta frequencies, in agreement with the fact that major long-range FF projections originate nearly exclusively from superficial layers, and FB from infragranular layers. Further, we note that gamma frequencies are generally associated with cortical activation, e.g. a visual stimulus or optogenetic activation, whereas alpha and beta frequencies are not clearly associated with a FF stimulus drive, consistent with the suggestion that FF provide the major driving influence (Covic and Sherman, 2011; De Pasquale and Sherman, 2011).

Future work will need to specifically address the nature of layer-specific functional interactions for individual FF and FB projections. The dual counterstream architecture postulates that a prominent short-range FB projection originates from L2 in the higher area. Consequently, we predict that FB from L2 is particularly strong at gamma-frequencies. Likewise, L5 is postulated to have a short-range FF projection, and to exhibit strong oscillations at alpha/beta frequencies. Hence, based on the dual counterstream architecture we predict a greater diversity of functional interactions than suggested by previous work, the elucidation of which will require high-density recording from all layers simultaneously across multiple cortical areas.

6. Diversity of FB pathways and their function in neural computation

In this section, we consider the possible functions of cortical FB and hierarchical organization in information processing. A large body of physiological studies has shown that FF pathways ascending the hierarchy generate increasingly complex representations of the world in higher areas, leading to the large range of receptive field properties observed at different levels of the hierarchy. Thus, at its core, convergent FF projections carry information from the outside world, and allow this information to be gradually transformed to low-dimensional representations that can be exploited for behavior. In this respect, it is worthwhile noting that the recent success of deep neural network architectures in solving complex tasks similarly demonstrates the power of FF transformations in computation (LeCun et al., 2015; Richards et al., 2019).

In contrast to FF-pathways, the neurobiology of the significantly *more* numerous FB pathways (Markov et al., 2014a) remains elusive, forming a major impediment to understanding the brain. A clearly defined role of FB connections is in attention, but FB pathways are likely critical in a host of complex operations including: the comparison of internally generated predictions of sensory input with actual inputs; imagining sensory inputs associated with a concept; carrying out mental simulations; and gating synaptic plasticity.

An early conceptualization of hierarchical processing in the cortex conceived of FF pathways driving target areas, and in contrast FB pathways merely exerting a modulatory influence (Klink et al., 2017), however, some researchers hold a more nuanced view (Bastos et al., 2012). Indeed, simple dichotomy of the roles of FF and FB pathways is difficult to reconcile with the multiple physiological effects that are imputed to FB control. For example, in the case of imagination, FB is conceived to *enhance* neural activity; by contrast in the case of filtering out self-generated sensory inputs, FB activity is expected to *suppress* neural activity. These forms of enhancement and suppression represent essentially distinct computational operations: a central concept is that of *gain modulation*, where an existing sensory representation is preserved, but in essence multiplied or divided, as in attentional mechanisms (McAdams and Maunsell, 1999). However, in the case of imagery, one expects FB to *"write-in"* a pattern of neural activity, i.e. operate a *driving* process, or alternatively selectively modulate the activity of specific spontaneously active cell assemblies. In the case of *cancelling out* self-generated sensory inputs through FB (as in self-tickling), FB activity is thought to be *subtractive* (Bastos et al., 2012). Finally, FB activity has been conceived to mediate *error* signals, playing a key role in shaping perceptual learning and synaptic plasticity. The notion of FB as a "swiss-army-knife" contrasts with FF processing which is essentially homogeneous and driving, as captured by the architecture of deep neural networks. These considerations underline the diversity of FB processes, which could be mediated by distinct neural circuits. In particular, we hypothesize that laminar and distance-determined diversity of FB pathways will exhibit anatomo-functional properties that characterize the cortical circuits underlying the diverse global influences engaged in different cognitive tasks. Given the diversity of FB pathways, and the many functions in which FB is implicated, it is a daunting task to develop a unified theory of the function of cortical FB. Yet, our understanding of the brain depends crucially on the development of precise theories of cortical FB.

The core feature of FB that distinguishes it from FF is that its projections are divergent; i.e. they project from few to many neurons. Interestingly, divergent projections are a core feature of the most popular kind of artificial neural network architectures, which are also rapidly becoming a mainstream model of sensory processing in the brain (LeCun et al., 2015; Richards et al., 2019). In feedforward (deep) neural networks, divergent error signals lead to an adjustment of synaptic weights of FF projections ("backprop"). In other words, in FF (deep) neural networks, the exclusive role of FB is to improve the data transformations implemented by the FF projections. For biological organism, error signals could be provided for instance by

multi-sensory signals or reward signals. However, it is an open question how FB would be able to adjust synaptic weights of FF projections (Whittington and Bogacz, 2019). A candidate pathway is the multiple FB projections converging onto L1 where they impact the distal dendrites of pyramidal neurons, activating non-linear NMDA-R-dependent dendritic integration mechanisms and voltage-gated calcium channels. Indeed, a recent study provides evidence that top-down FB to L1 might indeed be involved in perceptual learning in a primary sensory area: With reward reinforcement, mice rapidly learn a behavioral task in which their response is contingent on electric-current stimulation of S1. However, when L1 projections from perirhinal cortex to S1 are inhibited, mice fail to learn the same task, suggesting that top-down FB is instructive for learning (Doron et al., 2019). Another candidate pathway to modulate plasticity is the FB projection to VIP+ and SOM+ interneurons, given that SOM+ neurons can gate plasticity on the dendrites of pyramidal neurons (Batista-Brito et al., 2018).

There are major challenges at a conceptual level with the notion that FB signals transmit errors. In particular, the above mentioned learning experiment is in essence a supervised learning model, in the sense that FF networks are trained to make specific sensory decisions (e.g. recognizing a red apple as a red apple) based on some supervised feedback (e.g. multisensory: someone telling you it is a red apple; or reward: learning that red apples are delicious). However, it is not clear whether this kind of feedback would be sufficient for sensory learning. In the next section, we consider an alternative view on FB connections, namely that of a top-down generative network, in which divergent FB connections generate high-dimensional sensory representations starting from low-dimensional representations in higher brain areas.

7. Top down pathways constitute multiple generative networks?

In recent years the idea has emerged that top-down connections may have a generative function that can play an important role in generating sensory representations (Bastos et al., 2012; Hinton, 2007; Kosslyn, 1994; Mumford, 1992; Senden et al., 2019). In FF visual processing, high-dimensional sensory representations such as an image are sequentially transformed into low-dimensional representations such as object categories, represented at higher hierarchical levels. Conceivably FB pathways *invert* this process by generating high-dimensional representations starting from low-dimensional variables (Hinton, 2007). We refer to such pathways as top-down generative networks. Whereas the FF projections in convolutional networks create a convergence of information from many to few, in generative networks information is relayed by divergent projections from few to many. For instance, the perception of a red apple depends on a transformation of the image of a red apple (represented by many neurons) into high-level representations in the temporal lobe (represented by few neurons). However, if we imagine a red apple, processing should start from high-level representations (few neurons) and generate a low level neural representation of the image of a red apple (represented by many neurons).

Links between visual processing in deep artificial neural networks and the brain have been extended in recent years to cover putative roles of FB connections, and have started to involve generative neural network models (Bashivan et al., 2019; Hahn et al., 2019; Kietzmann et al., 2019; Nayebi et al., 2018). FB may enable approximate, probabilistic simulations to make robust and fast inferences in complex natural scenes where crucial information is unobserved (Battaglia et al., 2013). Analogues of mental simulation and imagery play an important role in model-based reinforcement learning (Hamrick, 2019). Moreover, the most powerful generative neural networks in machine learning such as GANs (generative adversarial network) and VAEs (variational autoencoder) have evolved substantially away from older and less efficient models for generative neural networks, raising the question as to what generative networks the brain uses.

An influential model of brain function that incorporates the notion of generative networks is the predictive coding framework. Predictive coding proposes that FB pathways transmit precise top-down reconstructions of sensory inputs and FF pathways signal reconstruction errors (Bastos et al., 2012; Mumford, 1992; Rao and Ballard, 1999). As discussed above in Section 5, in FF neural networks, error signals are thought to flow along FB pathways from high to low hierarchical levels. By contrast, predictive coding postulates that error signals do not flow down, but instead *up* the hierarchy. Error signals are postulated to be generated by the comparison (e.g. through subtraction) of FF inputs and FB predictions. The function of these error signals is to update information stored at high levels in the hierarchy, leading to the formation of better latent, generative models of the world, embedding a self-supervised learning scheme that minimizes surprise. Many studies have shown that cortical activity is modulated by sensory predictions or expectation, with enhanced activity for surprising stimuli (Bastos et al., 2012; de Lange et al., 2018), although factors like adaptation and bottom-up attention or salience (Li, 2002) (Zhaoping Li) could provide alternative interpretations for experimental findings. Hence, it remains unknown whether FF projections indeed carry *error signals* resulting from a comparison between FF and FB predictions (from the previous upper area) that can be understood as a precise mathematical operation (e.g. subtraction).

Most of the research in the framework of predictive coding has focused on the modulation of activity in lower areas by expectations or predictions induced by some behavioral task or stimulus repetition (Bastos et al., 2012; de Lange et al., 2018), however, little research has focused on testing whether FB connections in the brain are the substrate of a top-down generative network. The dual stream counterstream architecture suggests several features that are congruent with the hypothesis of top-down generative networks: *(1)* the convergence of cortical FF connections in the sensory stream is mirrored by the divergence of FB connections; *(2)* source populations of FF and FB pathways are completely separate, which has been recognized as a key requirement enabling distinct functionalities of generative top-down networks (Friston, 2018; Markov et al., 2014b; Shipp, 2016) *(3)* on average throughout the cortex there are twice as many FB pathways than FF projections to a given area. Studies in which human subjects are cued to generate a sensory percept also provide evidence for top-down generative networks in the cortex (Emmerling et al., 2016; Naselaris et al., 2015; Senden et al., 2019; Slotnick et al., 2005; Thirion et al., 2006).

While predictive coding assigns a relatively restricted role to top-down generative networks in terms of transmitting sensory predictions, they may play distinct functional roles in specific cognitive functions such as mental simulation, imagery or feature attention. An attractive idea of the generative top-down network hypothesis is that all of these functions could be subserved by a relatively small number of anatomical FB pathways implementing a function-specific generative network. This network would then interact with distinct cellular components in individual target areas in order to interact in different ways with ongoing ascending FF activity. As an example, we can take the processes of *imagination, predictive processing and attention.* In the case of *imagination* (e.g. thinking of a red apple), generative networks are expected to drive activity in lower areas based on the activation of neurons in higher areas; this effect can occur in the absence of any sensory stimulation. In the case of *predictive processing* (e.g. walking to the kitchen and expecting to see a red apple in the fruit basket, but not in the sink), generative networks may cause a reduction of neural activity in case a predicted stimulus occurs, whereas non-predicted stimuli would not be suppressed by top-down predictions. Finally, in the case of attention (e.g. searching for a red apple in the kitchen), generative networks may lead to an amplification of sensory activity when we find the stimulus that we were seeking.

Examining the dual counterstream suggests a possible division of labor between L2 and L6 FB projections: L2 FB and L3 FF projections exhibit common features that distinguish them from L6 FB. L2 FB and L3FF are short distance, topographically organized and exhibit low rates of bifurcation; contrasting with L6 FB which are long-distance, diffuse and have high rates of bifurcation. Thus, the L2 FB system may mirror the L3 FF system and implement a generative top-down network in which high-dimensional sensory representations can be generated through sequential stages, starting from higher brain areas. The L6 FB pathway, on the other hand, may determine the way in which the L2 generative network interacts with the local microcircuit, sending contextual signals that reflect behavioral goals and reward signals. Based on this hypothesis, we predict that L6 FB has more modulatory effects that it exerts, for example, via targeting the apical L1 dendrites as well as GABAergic interneurons such as SOM+ and VIP+ interneurons that modulate the activity of local pyramidal neurons (Batista-Brito et al., 2018). Testing this hypothesis will require parallel anatomical and physiological investigations. Optogenetic techniques in non-human primates could allow the injection of precise spatiotemporal activation patterns into specific laminar compartments of higher brain areas, combined with physiological measurements of activity in lower brain areas.

Box 1

Dual counterstream features	**Functional and structural correlates**
(1) Source populations of FF and FB pathways are completely separate, which has been recognized as a key requirement enabling distinct functionalities of generative top-down networks (Friston, 2018). A core feature of the dual counterstream architecture is that despite the ubiquity of bifurcation (Kennedy and Bullier, 1985), in no layer do individual neurons in FF and FB pathways possess both up and downstream collaterals (Markov et al., 2014b). Similar findings hold for mouse (Berezovskii et al., 2011). This indicates that FF and FB cells indeed constitute distinct populations.	Molecular characterization of FF and FB neurons is very much on the agenda. This would lead to the development of markers of these two projection types and hold the promise of the development of genetic tools for independent manipulation of different FB pathways.
(2) Large variability in the laminar configuration of FB pathways. FF connections are highly stereotypical, while FB projections show a large variability in their laminar origins and targets. Retrograde tracer in a midlevel target area labels up- and downstream areas with different proportions of supragranular neurons according to their hierarchical distance (Fig 2b). These laminar distributions of FF and FB neurons constitute their signatures that allow areas to be ranked in the Felleman and Van Essen hierarchy. Importantly, the different signatures of hierarchical distance reflect the changing laminar composition of the long-distance inputs to an area, meaning that "hierarchy" refers to the distance-dependent laminar-constrained integration of FF and FB inputs (Barone et al., 2000; Markov et al., 2014b) and signals (Bastos et al., 2015b; Michalareas et al., 2016) into the canonical microcircuit.	The multiplicity of the FB pathways in terms of laminar origins and targets over different distances suggest that compared to the singularity of FF pathways, individual FB pathways come in different flavors and fulfill different functions. These different FB pathways need to be investigated in human and NHP in high-field, laminar resolution fMRI and in parallel using invasive electrophysiology in NHP. These functional investigations are of particular relevance to the supragranular counterstream given the unique features of the Primate supragranular layers which are generated by a primate-specific germinal zone (OSVZ) (Smart et al., 2002), that exhibits complex cell lineages (Lukaszewicz et al., 2005) that we have hypothesized generate unique cell features in primates (Dehay et al., 2015) (Harris and Shepherd, 2015). These considerations support the notion that the two FB pathways (one in the supra- and one in infragranular layers) will have distinct functional roles in generative networks.
(3) FB and FF are not serially organized. Computational modelling studies e.g. (Bastos et al., 2012) invariably assume a serial hierarchical organization (Fig 12c) whereas in fact most areas receive and project to most other areas (Markov et al., 2014b).	The non-serial nature of inter-areal connectivity raises difficulty for ongoing attempts at large-scale computational modeling that needs to be given further attention.

(5) Lamination The dual counterstream architecture explicitly links pathways to layers, which is in-line with the increasing importance attached to cortical lamination and connectivity (Senzai, 2019). (l): effects on topography of FB. In addition to the low divergence-convergence values of supragranular layers (L2 FB and L3FF), and the high divergence-convergence values of infragranular layers (L5 FF and L6FB), high-rates of bifurcation by L6/L5 ensures innervation of multiple areas contrasting with and low levels of bifurcation by L2/L3 neurons (Kennedy and Bullier, 1985).	There are two interrelated issues here. Present understating of inter-areal connectivity in NHP, crucially lacks insight into the laminar restricted connectivity of these pathways. This requires using viral tracers in order to obtain precise information on the connectivity of individual pathways over different distances.
(6) Differences of FB and FF targets. The L3 FF projections primarily target upstream interneurons in L4. Presently we do not know the cellular targets of L2 FB projections although there is some suggestion that they could principally target L2 FB neurons in downstream areas, leading to long inter-areal FB chains. In parallel with differences in FF and FB cellular targets, do the cell targets change (and how) as a function of connection distance, possibly bringing a solution to addressing the problem raised in point (3)?	Laminar restricted connectivity to different cell types needs to be investigated in rodents and primates using next generation of viral tracers.
(7) FB show distinct development strategies. Differences in functionality are expected to require different developmental programs, which is indeed the case for FF and FB pathways. FF pathways develop precociously and exhibit directed-growth; FB pathway formation is delayed well into the postnatal period and exhibits diffuse growth followed by pruning (Barone et al., 1995; Barone et al., 1996; Kennedy et al., 1989).	These observations invite the investigation of inter-areal processing in NHP at different developmental periods and suggest that high-field, laminar resolution fMRI in infants and adults could reveal important developmental processes.

8. Conclusion.

We have reviewed evidence that inputs to a cortical area sample the cortical sheet in a principled manner defined by the differential space constants of the distance rules governing the individual cortical layers. This approach to understanding hierarchy is anchored in the recognition that it is the activity and connectivity linking neurons across the cortex that will ultimately reveal the process underlying the dynamics of cortical function. Link based investigation is complemented by characterization of the nodes. Helen Barbas pioneered the structural model, which shows that laminar differentiation allows hierarchical ranking of cortical areas that correlates well with connectivity patterns (Barbas, 2015). The structural model has proved to be extremely powerful because it links early observations on the gradual variations of cytoarchitecture and myeloarchitecture (Sanides, 1972) with graded changes in laminar thickness, neuron density and size. This has opened the interpretation of large-scale

models of the cortex to investigation with non-invasive imaging techniques that can be applied to the human brain (Burt et al., 2018; Margulies et al., 2016; Paquola et al., 2019).

The central argument of this review is that cortical hierarchy can be usefully thought of as an expression of the cortical input requirements of the local cortical circuit that in terms of synaptic mass constitutes the powerhouse of the cortex. Understanding the cellular mechanisms underlying hierarchical processing require investigations of hierarchy in terms of the laminar restricted connectivity and physiology that we have advocated in this review (Box 1). It is nearly 15 years since Jean Bullier posed the question "What is fed back?" (Bullier, 2006). The multiplicity of FB pathways and the complexity of their proposed functions were deep issues that he felt needed to be addressed. In the last 15 years there has been a spectacular development of three classes of techniques that allow us to address Jean Bullier's question. Firstly, optogenetics holographic stimulation makes it possible to address causation (Carrillo-Reid et al., 2019; Marshel et al., 2019), thereby addressing how activation of a given FB pathway influences a particular cognitive task. Secondly, viral tracing allows cell-type and laminar-constrained connectivity (El-Shamayleh et al., 2016; Nassi et al., 2015) making it possible to resolve the dual counterstream architecture. Thirdly, high-resolution fMRI allows single-layer resolution in the human brain (Kemper et al., 2018). The key feature will be to examine FB modulation of cognitive tasks in animal models that can, in parallel, be applied in humans where perceptual consequences can be reported (Kok et al., 2016; Schneider et al., 2019). These combined approaches will address the complexity of the interaction of descending generative networks with the local microcircuit (Haeusler and Maass, 2007) allowing computational modeling of top-down information flow.

Acknowledgments.
Funding gratefully acknowledged by XJW (ONR Grant N00014-17-1-2041, US National Institutes of Health NIH grant 062349, Simons Collaboration on the Global Brain program grant 543057SPI) ; KK (DUAL_STREAM ANR-19-CE37) ; MV (ERC Starting Grant – SPATEMP, BINDABMF -Bundesministerium Forschung) ; HK (LABEX CORTEX ANR-11-LABX-0042; Université de Lyon ANR-11-IDEX-0007), A2P2MC ANR-17-NEUC-0004, CORTICITY ANR-17-HBPR-0003, SCUSI, Région Auvergne-Rhône-Alpes 1700933701.

Author contribution. Data acquisition JV, LM; Analysis of data JV, LM, KK; Statistical modeling of hierarchy KK; Wrote the paper XJW, KK, MV, HK; All authors revised and edited the completed document; Proposed the study HK

References

Ardid, S., Wang, X.J., 2013. A tweaking principle for executive control: neuronal circuit mechanism for rule-based task switching and conflict resolution. J Neurosci 33, 19504-19517.

Armstrong, K.M., Fitzgerald, J.K., Moore, T., 2006. Changes in visual receptive fields with microstimulation of frontal cortex. Neuron 50, 791-798.

Badre, D., D'Esposito, M., 2007. Functional magnetic resonance imaging evidence for a hierarchical organization of the prefrontal cortex. J Cogn Neurosci 19, 2082-2099.

Badre, D., D'Esposito, M., 2009. Is the rostro-caudal axis of the frontal lobe hierarchical? Nat Rev Neurosci 10, 659-669.

Barbas, H., 2015. General cortical and special prefrontal connections: principles from structure to function. Annu Rev Neurosci 38, 269-289.

Barone, P., Batardiere, A., Knoblauch, K., Kennedy, H., 2000. Laminar distribution of neurons in extrastriate areas projecting to visual areas V1 and V4 correlates with the hierarchical rank and indicates the operation of a distance rule. J Neurosci 20, 3263-3281.

Barone, P., Dehay, C., Berland, M., Bullier, J., Kennedy, H., 1995. Developmental remodeling of primate visual cortical pathways. Cereb Cortex 5, 22-38.

Barone, P., Dehay, C., Berland, M., Kennedy, H., 1996. Role of directed growth and target selection in the formation of cortical pathways: prenatal development of the projection of area V2 to area V4 in the monkey. J Comp Neurol 374, 1-20.

Barth, A.L., Poulet, J.F., 2012. Experimental evidence for sparse firing in the neocortex. Trends Neurosci 35, 345-355.

Bashivan, P., Kar, K., DiCarlo, J.J., 2019. Neural population control via deep image synthesis. Science 364.

Bastos, A.M., Litvak, V., Moran, R., Bosman, C.A., Fries, P., Friston, K.J., 2015a. A DCM study of spectral asymmetries in feedforward and feedback connections between visual areas V1 and V4 in the monkey. Neuroimage 108, 460-475.

Bastos, A.M., Loonis, R., Kornblith, S., Lundqvist, M., Miller, E.K., 2018. Laminar recordings in frontal cortex suggest distinct layers for maintenance and control of working memory. Proc Natl Acad Sci U S A 115, 1117-1122.

Bastos, A.M., Usrey, W.M., Adams, R.A., Mangun, G.R., Fries, P., Friston, K.J., 2012. Canonical microcircuits for predictive coding. Neuron 76, 695-711.

Bastos, A.M., Vezoli, J., Bosman, C.A., Schoffelen, J.M., Oostenveld, R., Dowdall, J.R., De Weerd, P., Kennedy, H., Fries, P., 2015b. Visual Areas Exert Feedforward and Feedback Influences through Distinct Frequency Channels. Neuron 85, 390-401.

Batista-Brito, R., Zagha, E., Ratliff, J.M., Vinck, M., 2018. Modulation of cortical circuits by top-down processing and arousal state in health and disease. Curr Opin Neurobiol 52, 172-181.

Battaglia, P.W., Hamrick, J.B., Tenenbaum, J.B., 2013. Simulation as an engine of physical scene understanding. Proc Natl Acad Sci U S A 110, 18327-18332.

Berezovskii, V.K., Nassi, J.J., Born, R.T., 2011. Segregation of feedforward and feedback projections in mouse visual cortex. J Comp Neurol 519, 3672-3683.

Betizeau, M., Cortay, V., Patti, D., Pfister, S., Gautier, E., Bellemin-Menard, A., Afanassieff, M., Huissoud, C., Douglas, R.J., Kennedy, H., Dehay, C., 2013. Precursor diversity and complexity of lineage relationships in the outer subventricular zone (OSVZ) of the primate. Neuron 80, 442-457.

Binzegger, T., Douglas, R.J., Martin, K.A., 2004. A quantitative map of the circuit of cat primary visual cortex. J Neurosci 24, 8441-8453.

Binzegger, T., Douglas, R.J., Martin, K.A., 2009. Topology and dynamics of the canonical circuit of cat V1. Neural Netw 22, 1071-1078.

Bollimunta, A., Chen, Y., Schroeder, C.E., Ding, M., 2008. Neuronal mechanisms of cortical alpha oscillations in awake-behaving macaques. J Neurosci 28, 9976-9988.

Bonnefond, M., Kastner, S., Jensen, O., 2017. Communication between Brain Areas Based on Nested Oscillations. eNeuro 4.

Buffalo, E.A., Fries, P., Landman, R., Buschman, T.J., Desimone, R., 2011. Laminar differences in gamma and alpha coherence in the ventral stream. Proc Natl Acad Sci U S A 108, 11262-11267.

Bullier, J., 2006. What is Fed Back? In: van Hemmen, J.L., Sejnowski, T.J. (Eds.), 23 Problems in Systems Neuroscience. Oxford University Press USA, pp. 103-132.

Burns, S.P., Xing, D., Shapley, R.M., 2011. Is gamma-band activity in the local field potential of V1 cortex a "clock" or filtered noise? J Neurosci 31, 9658-9664.

Burt, J.B., Demirtas, M., Eckner, W.J., Navejar, N.M., Ji, J.L., Martin, W.J., Bernacchia, A., Anticevic, A., Murray, J.D., 2018. Hierarchy of transcriptomic specialization across human cortex captured by structural neuroimaging topography. Nat Neurosci 21, 1251-1259.

Buzsaki, G., Wang, X.J., 2012. Mechanisms of gamma oscillations. Annu Rev Neurosci 35, 203-225.

Cahalane, D.J., Charvet, C.J., Finlay, B.L., 2014. Modeling local and cross-species neuron number variations in the cerebral cortex as arising from a common mechanism. Proc Natl Acad Sci U S A 111, 17642-17647.

Cardin, J.A., Carlen, M., Meletis, K., Knoblich, U., Zhang, F., Deisseroth, K., Tsai, L.H., Moore, C.I., 2009. Driving fast-spiking cells induces gamma rhythm and controls sensory responses. Nature 459, 663-667.

Carrillo-Reid, L., Han, S., Yang, W., Akrouh, A., Yuste, R., 2019. Controlling Visually Guided Behavior by Holographic Recalling of Cortical Ensembles. Cell 178, 447-457 e445.

Chaudhuri, R., Knoblauch, K., Gariel, M.A., Kennedy, H., Wang, X.J., 2015. A Large-Scale Circuit Mechanism for Hierarchical Dynamical Processing in the Primate Cortex. Neuron 88, 419-431.

Choi, E.Y., Drayna, G.K., Badre, D., 2018. Evidence for a Functional Hierarchy of Association Networks. J Cogn Neurosci 30, 722-736.

Cossell, L., Iacaruso, M.F., Muir, D.R., Houlton, R., Sader, E.N., Ko, H., Hofer, S.B., Mrsic-Flogel, T.D., 2015. Functional organization of excitatory synaptic strength in primary visual cortex. Nature.

Covic, E.N., Sherman, S.M., 2011. Synaptic properties of connections between the primary and secondary auditory cortices in mice. Cereb Cortex 21, 2425-2441.

Cragg, B.G., 1969. The topography of the afferent projections in the circumstriate visual cortex of the monkey studied by the Nauta method. Vision Res 9, 733-747.

Crick, F., Koch, C., 1998. Constraints on cortical and thalamic projections: the no-strong-loops hypothesis. Nature 391, 245-250.

Crochet, S., Poulet, J.F., Kremer, Y., Petersen, C.C., 2011. Synaptic mechanisms underlying sparse coding of active touch. Neuron 69, 1160-1175.

D'Souza, R., Wang, Q., Ji, W., Meier, A., Kennedy, H., Knoblauch, K., Burkhalter, A., 2020. Canonical and noncanonical features of the mouse visual cortical hierarchy. bioRxiv, 2020.2003.2030.016303.

da Costa, N.M., Martin, K.A., 2010. Whose Cortical Column Would that Be? Front Neuroanat 4, 16.

de Lange, F.P., Heilbron, M., Kok, P., 2018. How Do Expectations Shape Perception? Trends Cogn Sci 22, 764-779.

De Pasquale, R., Sherman, S.M., 2011. Synaptic properties of corticocortical connections between the primary and secondary visual cortical areas in the mouse. J Neurosci 31, 16494-16506.

Dehay, C., Kennedy, H., Kosik, K.S., 2015. The Outer Subventricular Zone and Primate-Specific Cortical Complexification. Neuron 85, 683-694.

Doron, G., Shin, J.N., Takahashi, N., Bocklisch, C., Skenderi, S., Drüke, M., de Mont, L., Toumazo, M., von Heimendahl, M., Brecht, M., Naud, R., Larkum, M.E., 2019. Perirhinal input to neocortical layer 1 controls learning. bioRxiv, 713883.

Douglas, R.J., Koch, C., Mahowald, M., Martin, K.A., Suarez, H.H., 1995. Recurrent excitation in neocortical circuits. Science 269, 981-985.

Douglas, R.J., Martin, K.A., 1991. A functional microcircuit for cat visual cortex. J Physiol 440, 735-769.

Douglas, R.J., Martin, K.A., 2007a. Mapping the matrix: the ways of neocortex. Neuron 56, 226-238.

Douglas, R.J., Martin, K.A., 2007b. Recurrent neuronal circuits in the neocortex. Curr Biol 17, R496-500.

Douglas, R.J., Martin, K.A.C., Whitteridge, D., 1989. A canonical microcircuit for neocortex. Neural Comput 1, 480-488.

El-Shamayleh, Y., Ni, A.M., Horwitz, G.D., 2016. Strategies for targeting primate neural circuits with viral vectors. J Neurophysiol 116, 122-134.

Emmerling, T.C., Zimmermann, J., Sorger, B., Frost, M.A., Goebel, R., 2016. Decoding the direction of imagined visual motion using 7T ultra-high field fMRI. Neuroimage 125, 61-73.

Ercsey-Ravasz, M., Markov, N.T., Lamy, C., Van Essen, D.C., Knoblauch, K., Toroczkai, Z., Kennedy, H., 2013. A predictive network model of cerebral cortical connectivity based on a distance rule. Neuron 80, 184-197.

Felleman, D.J., Van Essen, D.C., 1991. Distributed hierarchical processing in the primate cerebral cortex. Cereb Cortex 1, 1-47.

Ferster, D., Chung, S., Wheat, H., 1996. Orintation delectivity of thalamic input to simple cells of cat visual cortex. Nature 380, 249-252.

Friston, K., 2018. Does predictive coding have a future? Nat Neurosci 21, 1019-1021.

Garcia-Marin, V., Kelly, J.G., Hawken, M.J., 2019. Major Feedforward Thalamic Input Into Layer 4C of Primary Visual Cortex in Primate. Cereb Cortex 29, 134-149.

Geschwind, D.H., Rakic, P., 2013. Cortical evolution: judge the brain by its cover. Neuron 80, 633-647.

Gilbert, C.D., Li, W., 2013. Top-down influences on visual processing. Nat Rev Neurosci 14, 350-363.

Goulas, A., Uylings, H.B., Stiers, P., 2014. Mapping the hierarchical layout of the structural network of the macaque prefrontal cortex. Cereb Cortex 24, 1178-1194.

Gregoriou, G.G., Gotts, S.J., Desimone, R., 2012. Cell-type-specific synchronization of neural activity in FEF with V4 during attention. Neuron 73, 581-594.

Gregoriou, G.G., Gotts, S.J., Zhou, H., Desimone, R., 2009. High-frequency, long-range coupling between prefrontal and visual cortex during attention. Science 324, 1207-1210.

Haeusler, S., Maass, W., 2007. A statistical analysis of information-processing properties of lamina-specific cortical microcircuit models. Cereb Cortex 17, 149-162.

Hahn, G., Ponce-Alvarez, A., Deco, G., Aertsen, A., Kumar, A., 2019. Portraits of communication in neuronal networks. Nat Rev Neurosci 20, 117-127.

Haider, B., Hausser, M., Carandini, M., 2013. Inhibition dominates sensory responses in the awake cortex. Nature 493, 97-100.

Hamrick, J.B., 2019. Analogues of mental simulation and imagination in deep learning. Curr Opin Behav Sci 29, 8-16.

Harris, K.D., Mrsic-Flogel, T.D., 2013. Cortical connectivity and sensory coding. Nature 503, 51-58.

Harris, K.D., Shepherd, G.M., 2015. The neocortical circuit: themes and variations. Nat Neurosci 18, 170-181.

Hasenstaub, A., Shu, Y., Haider, B., Kraushaar, U., Duque, A., McCormick, D.A., 2005. Inhibitory postsynaptic potentials carry synchronized frequency information in active cortical networks. Neuron 47, 423-435.

Hawkins, J., Blakeslee, S., 2004. On intelligence: How A New Understanding of the brain will lad to the creation of truely intelligent machines. Owl books.

Hilgetag, C.C., Goulas, A., 2020. 'Hierarchy' in the organization of brain networks. Philos Trans R Soc Lond B Biol Sci 375, 20190319.

Hilgetag, C.C., O'Neill, M.A., Young, M.P., 1996. Indeterminate organization of the visual system. Science 271, 776-777.

Hinton, G.E., 2007. Learning multiple layers of representation. Trends Cogn Sci 11, 428-434.

Hu, H., Gan, J., Jonas, P., 2014. Interneurons. Fast-spiking, parvalbumin(+) GABAergic interneurons: from cellular design to microcircuit function. Science 345, 1255263.
Hubel, D., 1995. Eye, brain and vision. Freeman and Co, New York.
Hubel, D.H., Wiesel, T.N., 1962. Receptive fields binocular interaction and functional architecture in the cat visual cortex. J Physiol 160, 106-154.
Hubel, D.H., Wiesel, T.N., 1977. Ferrier lecture. Functional architecture of macaque monkey visual cortex. Proc R Soc Lond B Biol Sci 198, 1-59.
Jouhanneau, J.S., Kremkow, J., Poulet, J.F.A., 2018. Single synaptic inputs drive high-precision action potentials in parvalbumin expressing GABA-ergic cortical neurons in vivo. Nat Commun 9, 1540.
Kaas, J.H., Lin, C.S., 1977. Cortical projections of area 18 in owl monkeys. Vision Res 17, 739-741.
Kemper, V.G., De Martino, F., Emmerling, T.C., Yacoub, E., Goebel, R., 2018. High resolution data analysis strategies for mesoscale human functional MRI at 7 and 9.4T. Neuroimage 164, 48-58.
Kennedy, H., Bullier, J., 1985. A double-labeling investigation of the afferent connectivity to cortical areas V1 and V2 of the macaque monkey. J Neurosci 5, 2815-2830.
Kennedy, H., Bullier, J., Dehay, C., 1989. Transient projections from the superior temporal sulcus to area 17 in the newborn macaque monkey. Proc Natl Acad Sci USA 86, 8093-8097.
Kietzmann, T.C., Spoerer, C.J., Sorensen, L.K.A., Cichy, R.M., Hauk, O., Kriegeskorte, N., 2019. Recurrence is required to capture the representational dynamics of the human visual system. Proc Natl Acad Sci U S A 116, 21854-21863.
Klink, P.C., Dagnino, B., Gariel-Mathis, M.A., Roelfsema, P.R., 2017. Distinct Feedforward and Feedback Effects of Microstimulation in Visual Cortex Reveal Neural Mechanisms of Texture Segregation. Neuron 95, 209-220 e203.
Ko, H., Hofer, S.B., Pichler, B., Buchanan, K.A., Sjostrom, P.J., Mrsic-Flogel, T.D., 2011. Functional specificity of local synaptic connections in neocortical networks. Nature 473, 87-91.
Koechlin, E., Ody, C., Kouneiher, F., 2003. The architecture of cognitive control in the human prefrontal cortex. Science 302, 1181-1185.
Kok, P., Bains, L.J., van Mourik, T., Norris, D.G., de Lange, F.P., 2016. Selective Activation of the Deep Layers of the Human Primary Visual Cortex by Top-Down Feedback. Curr Biol 26, 371-376.
Kosslyn, S.M., 1994. Image and Brain. MIT Press.
Kuypers, H.G.J.M., Szwarcbart, M.K., Mishkin, M., Rosvold, H.E., 1965. Occipitotemporal corticortical connections in the rhesus monkey. Exp Neurol 11, 245-262.
LeCun, Y., Bengio, Y., Hinton, G., 2015. Deep learning. Nature 521, 436-444.
Lee, W.C., Bonin, V., Reed, M., Graham, B.J., Hood, G., Glattfelder, K., Reid, R.C., 2016. Anatomy and function of an excitatory network in the visual cortex. Nature 532, 370-374.
Lesnoff, M., Lancelot, R., 2012. aod: Analysis of Overdispersed Data. R package version 1.3 http://cran.r-project.org/package=aod.
Li, Z., 2002. A saliency map in primary visual cortex. Trends Cogn Sci 6, 9-16.
Lien, A.D., Scanziani, M., 2013. Tuned thalamic excitation is amplified by visual cortical circuits. Nat Neurosci 16, 1315-1323.
Lukaszewicz, A., Savatier, P., Cortay, V., Giroud, P., Huissoud, C., Berland, M., Kennedy, H., Dehay, C., 2005. G1 phase regulation, area-specific cell cycle control, and cytoarchitectonics in the primate cortex. Neuron 47, 353-364.

Lund, J.S., Lund, R.D., Hendrickson, A.E., Bunt, A.H., Fuchs, A.F., 1975. The origin of efferent pathways from the primary visual cortex of the macaque monkey as shown by retrograde transport of horseradish peroxydase. J Comp Neurol 164, 287-304.

Magrou, L., Barone, P., Markov, N.T., Killackey, H.P., Giroud, P., Berland, M., Knoblauch, K., Dehay, C., Kennedy, H., 2018. How Areal Specification Shapes the Local and Interareal Circuits in a Macaque Model of Congenital Blindness. Cereb Cortex 28, 3017-3034.

Margulies, D.S., Ghosh, S.S., Goulas, A., Falkiewicz, M., Huntenburg, J.M., Langs, G., Bezgin, G., Eickhoff, S.B., Castellanos, F.X., Petrides, M., Jefferies, E., Smallwood, J., 2016. Situating the default-mode network along a principal gradient of macroscale cortical organization. Proc Natl Acad Sci U S A 113, 12574-12579.

Markov, N.T., Ercsey-Ravasz, M., Van Essen, D.C., Knoblauch, K., Toroczkai, Z., Kennedy, H., 2013. Cortical high-density counter-stream architectures. Science 342, 1238406.

Markov, N.T., Ercsey-Ravasz, M.M., Ribeiro Gomes, A.R., Lamy, C., Magrou, L., Vezoli, J., Misery, P., Falchier, A., Quilodran, R., Gariel, M.A., Sallet, J., Gamanut, R., Huissoud, C., Clavagnier, S., Giroud, P., Sappey-Marinier, D., Barone, P., Dehay, C., Toroczkai, Z., Knoblauch, K., Van Essen, D.C., Kennedy, H., 2014a. A weighted and directed interareal connectivity matrix for macaque cerebral cortex. Cereb Cortex 24, 17-36.

Markov, N.T., Misery, P., Falchier, A., Lamy, C., Vezoli, J., Quilodran, R., Gariel, M.A., Giroud, P., Ercsey-Ravasz, M., Pilaz, L.J., Huissoud, C., Barone, P., Dehay, C., Toroczkai, Z., Van Essen, D.C., Kennedy, H., Knoblauch, K., 2011. Weight Consistency Specifies Regularities of Macaque Cortical Networks. Cereb Cortex 21, 1254-1272.

Markov, N.T., Vezoli, J., Chameau, P., Falchier, A., Quilodran, R., Huissoud, C., Lamy, C., Misery, P., Giroud, P., Barone, P., Dehay, C., Ullman, S., Knoblauch, K., Kennedy, H., 2014b. The Anatomy of Hierarchy: Feedforward and feedback pathways in macaque visual cortex. J Comp Neurol 522, 225-259.

Marshel, J.H., Kim, Y.S., Machado, T.A., Quirin, S., Benson, B., Kadmon, J., Raja, C., Chibukhchyan, A., Ramakrishnan, C., Inoue, M., Shane, J.C., McKnight, D.J., Yoshizawa, S., Kato, H.E., Ganguli, S., Deisseroth, K., 2019. Cortical layer-specific critical dynamics triggering perception. Science 365.

Martinez-Millan, L., Hollander, H., 1975. Cortico-cortical projections from striate cortex of the squirrel monkey (saimiri sciureus). A radioautographic study. Brain Res 83, 405-417.

McAdams, C.J., Maunsell, J.H., 1999. Effects of attention on orientation-tuning functions of single neurons in macaque cortical area V4. J Neurosci 19, 431-441.

Michalareas, G., Vezoli, J., van Pelt, S., Schoffelen, J.M., Kennedy, H., Fries, P., 2016. Alpha-Beta and Gamma Rhythms Subserve Feedback and Feedforward Influences among Human Visual Cortical Areas. Neuron 89, 384-397.

Moore, C.I., Carlen, M., Knoblich, U., Cardin, J.A., 2010. Neocortical interneurons: from diversity, strength. Cell 142, 189-193.

Moore, T., Armstrong, K.M., 2003. Selective gating of visual signals by microstimulation of frontal cortex. Nature 421, 370-373.

Mountcastle, V., 1995. The evolution of ideas concerning the function of the neocortex. Cerbral cortex 5, 289-295.

Mountcastle, V.B., 1957. Modality and topographic properties of single neurons of cat's somatic sensory cortex. J Neurophysiol 20, 408-434.

Mumford, D., 1992. On the computational architecture of the neocortex. II. The role of cortico-cortical loops. Biol Cybern 66, 241-251.

Naselaris, T., Olman, C.A., Stansbury, D.E., Ugurbil, K., Gallant, J.L., 2015. A voxel-wise encoding model for early visual areas decodes mental images of remembered scenes. Neuroimage 105, 215-228.

Nassi, J.J., Cepko, C.L., Born, R.T., Beier, K.T., 2015. Neuroanatomy goes viral! Front Neuroanat 9, 80.

Nayebi, A., Bear, D., Kubilius, J., Kar, K., Ganguli, S., Sussillo, D., DiCarlo, J.J., Yamins, D.L.K., 2018. Task-Driven convolutional recurrent models of the visual system. NIPS'18 Proceedings of the 32nd International Conference on Neural Information Processing Systems, pp. 5295-5306.

Paquola, C., Vos De Wael, R., Wagstyl, K., Bethlehem, R.A.I., Hong, S.J., Seidlitz, J., Bullmore, E.T., Evans, A.C., Misic, B., Margulies, D.S., Smallwood, J., Bernhardt, B.C., 2019. Microstructural and functional gradients are increasingly dissociated in transmodal cortices. PLoS Biol 17, e3000284.

Petersen, C.C., Crochet, S., 2013. Synaptic computation and sensory processing in neocortical layer 2/3. Neuron 78, 28-48.

Pike, F.G., Goddard, R.S., Suckling, J.M., Ganter, P., Kasthuri, N., Paulsen, O., 2000. Distinct frequency preferences of different types of rat hippocampal neurones in response to oscillatory input currents. J Physiol 529 Pt 1, 205-213.

Pouget, P., Stepniewska, I., Crowder, E.A., Leslie, M.W., Emeric, E.E., Nelson, M.J., Schall, J.D., 2009. Visual and motor connectivity and the distribution of calcium-binding proteins in macaque frontal eye field: implications for saccade target selection. Front Neuroanat 3, 2.

Rao, R.P., Ballard, D.H., 1999. Predictive coding in the visual cortex: a functional interpretation of some extra-classical receptive-field effects. Nat Neurosci 2, 79-87.

Richards, B.A., Lillicrap, T.P., Beaudoin, P., Bengio, Y., Bogacz, R., Christensen, A., Clopath, C., Costa, R.P., de Berker, A., Ganguli, S., Gillon, C.J., Hafner, D., Kepecs, A., Kriegeskorte, N., Latham, P., Lindsay, G.W., Miller, K.D., Naud, R., Pack, C.C., Poirazi, P., Roelfsema, P., Sacramento, J., Saxe, A., Scellier, B., Schapiro, A.C., Senn, W., Wayne, G., Yamins, D., Zenke, F., Zylberberg, J., Therien, D., Kording, K.P., 2019. A deep learning framework for neuroscience. Nat Neurosci 22, 1761-1770.

Richter, C.G., Coppola, R., Bressler, S.L., 2018. Top-down beta oscillatory signaling conveys behavioral context in early visual cortex. Sci Rep 8, 6991.

Rockland, K.S., Pandya, D.N., 1979. Laminar origins and terminations of cortical connections of the occipital lobe in the rhesus monkey. Brain Res 179, 3-20.

Roelfsema, P.R., de Lange, F.P., 2016. Early Visual Cortex as a Multiscale Cognitive Blackboard. Annu Rev Vis Sci 2, 131-151.

Sakata, S., Harris, K.D., 2009. Laminar structure of spontaneous and sensory-evoked population activity in auditory cortex. Neuron 64, 404-418.

Sanides, F., 1972. Representation in the cerebral cortex and its areal lamination patterns. In: Bourne, G.H. (Ed.), The structure and function of the nervous tissue. Academic Press, New York and London, pp. 329-453.

Schall, J.D., 2015. Visuomotor Functions in the Frontal Lobe. Annu Rev Vis Sci 1, 469-498.

Schneider, M., Kemper, V.G., Emmerling, T.C., De Martino, F., Goebel, R., 2019. Columnar clusters in the human motion complex reflect consciously perceived motion axis. Proc Natl Acad Sci U S A 116, 5096-5101.

Schumacher, F.K., Schumacher, L.V., Schelter, B.O., Kaller, C.P., 2019. Functionally dissociating ventro-dorsal components within the rostro-caudal hierarchical organization of the human prefrontal cortex. Neuroimage 185, 398-407.

Senden, M., Emmerling, T.C., van Hoof, R., Frost, M.A., Goebel, R., 2019. Reconstructing imagined letters from early visual cortex reveals tight topographic correspondence between visual mental imagery and perception. Brain Struct Funct 224, 1167-1183.

Senzai, Y., Fernandez, A., Buzaki, G. , 2019. Layer specific physiological features and interlaminar interactions in the primary visual cortex of the mouse. Neuron 101, 500-503.

Shipp, S., 2016. Neural Elements for Predictive Coding. Front Psychol 7, 1792.

Slotnick, S.D., Thompson, W.L., Kosslyn, S.M., 2005. Visual mental imagery induces retinotopically organized activation of early visual areas. Cereb Cortex 15, 1570-1583.

Smart, I.H., Dehay, C., Giroud, P., Berland, M., Kennedy, H., 2002. Unique morphological features of the proliferative zones and postmitotic compartments of the neural epithelium giving rise to striate and extrastriate cortex in the monkey. Cereb Cortex 12, 37-53.

Song, S., Sjostrom, P.J., Reigl, M., Nelson, S., Chklovskii, D.B., 2005. Highly nonrandom features of synaptic connectivity in local cortical circuits. PLoS Biol 3, e68.

Spatz, W.B., Tigges, J., Tigges, M., 1970. Subcortical projections, cortical associations, and some intrinsic interlaminar connections of the striate cortex in the squirrel monkey (saimiri). J Comp Neurol 140, 155-174.

Spyropoulos, G., Dowdall, J.R., Schölvinck, M.L., Bosman, C.A., Lima, B., Peter, A., Onorato, I., Klon-Lipok, J., Roese, R., Neuenschwander, S., Singer, W., Vinck, M., Fries, P., 2019. Gamma-cycle duration predicts instantaneous amplitude, spike rate and synchrony in macaque V1. bioRxiv, 793729.

Tang, S., Zhang, Y., Li, Z., Li, M., Liu, F., Jiang, H., Lee, T.S., 2018. Large-scale two-photon imaging revealed super-sparse population codes in the V1 superficial layer of awake monkeys. Elife 7.

Thirion, B., Duchesnay, E., Hubbard, E., Dubois, J., Poline, J.B., Lebihan, D., Dehaene, S., 2006. Inverse retinotopy: inferring the visual content of images from brain activation patterns. Neuroimage 33, 1104-1116.

Tigges, J., Spatz, W.B., Tigges, M., 1973. Reciprocal point-to-point connections between parastriate and striate cortex in the squirrel monkey (saimiri). J Comp Neurol 148, 481-490.

Treue, S., Maunsell, J.H., 1996. Attentional modulation of visual motion processing in cortical areas MT and MST. Nature 382, 539-541.

Tsodyks, M., Kenet, T., Grinvald, A., Arieli, A., 1999. Linking spontaneous activity of single cortical neurons and the underlying functional architecture. Science 286, 1943-1946.

Ullman, S., 1995. Sequence seeking and counter streams: a computational model for bidirectional information flow in the visual cortex. Cereb Cortex 5, 1-11.

Ullman, S., 2000. Sequence seeking and counter streams: A model for information flow in the visual cortex. High-Level Vision. Bradford / MIT Press.

Van Essen, D.C., Zeki, S., 1978. The topographic organization of rhesus monkey prestriate cortex. J Physiol 277, 193-226.

van Kerkoerle, T., Self, M.W., Dagnino, B., Gariel-Mathis, M.A., Poort, J., van der Togt, C., Roelfsema, P.R., 2014. Alpha and gamma oscillations characterize feedback and feedforward processing in monkey visual cortex. Proc Natl Acad Sci U S A 111, 14332-14341.

Vezoli, J., Falchier, A., Jouve, B., Knoblauch, K., Young, M., Kennedy, H., 2004. Quantitative analysis of connectivity in the visual cortex: extracting function from structure. Neuroscientist 10, 476-482.

Vinck, M., Bosman, C.A., 2016. More Gamma More Predictions: Gamma-Synchronization as a Key Mechanism for Efficient Integration of Classical Receptive Field Inputs with Surround Predictions. Front Syst Neurosci 10, 35.

Vinje, W.E., Gallant, J.L., 2000. Sparse coding and decorrelation in primary visual cortex during natural vision. Science 287, 1273-1276.

Wang, X.-J., Kennedy, H., 2016. Brain structure and dynamics across scales: in search of rules. Curr Opin Neurobiol 37, 92-98.

Wang, X.J., 2010. Neurophysiological and computational principles of cortical rhythms in cognition. Physiol Rev 90, 1195-1268.

Whittington, J.C.R., Bogacz, R., 2019. Theories of Error Back-Propagation in the Brain. Trends Cogn Sci 23, 235-250.

Willmore, B.D., Mazer, J.A., Gallant, J.L., 2011. Sparse coding in striate and extrastriate visual cortex. J Neurophysiol 105, 2907-2919.

Wong-Riley, M., 1978. Reciprocal connections between striate and prestriate cortex in the squirrel monkey as demonstrated by combined peroxydase histochemistry and autoradiography. Brain Res 147, 159-164.

York, G.K., 3rd, Steinberg, D.A., 2011. Hughlings Jackson's neurological ideas. Brain 134, 3106-3113.

Zeng, H., Shen, E.H., Hohmann, J.G., Oh, S.W., Bernard, A., Royall, J.J., Glattfelder, K.J., Sunkin, S.M., Morris, J.A., Guillozet-Bongaarts, A.L., Smith, K.A., Ebbert, A.J., Swanson, B., Kuan, L., Page, D.T., Overly, C.C., Lein, E.S., Hawrylycz, M.J., Hof, P.R., Hyde, T.M., Kleinman, J.E., Jones, A.R., 2012. Large-scale cellular-resolution gene profiling in human neocortex reveals species-specific molecular signatures. Cell 149, 483-496.

Zipser, K., Lamme, V.A., Schiller, P.H., 1996. Contextual modulation in primary visual cortex. J Neurosci 16, 7376-7389.

Figure Legends

Figure 1. Quantitative map of excitatory synapses between excitatory neurons of the local microcircuit in visual cortex (area 17) of the cat. The feedforward loop starts in layer 4, the major thalamic recipient layer and then extends to layers 2/3, 5 and 6 with recurrent inputs back to layer 4. This feedforward loop corresponds to a little less than half of synapses involved in self-innervation of individual cortical layers. X/Y refers to the component cells of the lateral geniculate nucleus, the major thalamic relay. The original canonical microcircuit is shown in figure 12b. L refers to layer. From (Binzegger et al., 2004) with permission.

Figure 2. Quantitative parameters characterizing the hierarchy. A: The laminar distribution of parent neurons in each pathway, referred to as SLN (fraction of supragranular neurons) is determined by high frequency sampling and quantitative analysis of labeling. Supra- and infragranular layer neurons contribute to both feedback and feedforward pathways, and their relative proportion is characteristic for each type of pathway. For a given injection there is a gradient of SLN of the labeled areas, between purely FF (SLN = 100%, all the parent neurons are in the supragranular layers) to purely FB (SLN = 0%, all the parent neurons in the infragranular layers) and a spectrum of intermediate proportions; **B**: All labeled areas can then be ordered by decreasing SLN values and this order is consistent with hierarchical order according to Felleman and Van Essen. SLN is thus used as an indicator of hierarchical distance between areas from the same injection (Barone et al., 2000; Vezoli et al., 2004); **C**: FLN (fraction of labeled neurons) indicates the relative strength of each pathway (in number of labeled neurons) compared to the total number of neurons that are labeled in the cortical hemisphere after the injection. It requires counting labeled neurons from sections spanning the whole brain, but gives insight into the weight of connections. Vezoli et al. (Vezoli et al., 2004) showed that short-distance connections have high FLN values, whereas the strength of connection decreases as physical distance between source and target areas increases.

Figure 3. Properties of nodes and links. Nodes have fixed properties, a, b, c which in turn fixes their order and any distance measure, d, calculated from these properties. b. Link properties depend on the relations between node pairs, ab, bc, ac. The distance measures, δ, for ab, and bc do not necessarily fix that for ac. The above graphs are unidirectional, but in bi-directional graphs the distances between nodes need not by symmetric.

Figure 4. Hierarchical scales. Suppose a hierarchical scale between areas A, B, C, D, with the ordering and distances as illustrated on the bottom line. We expect measures of distance to be consistent measured between any pairs of areas. For example, injections in areas A and B lead to distances defined with respect to each of these areas, i.e., distances AB (double headed grey arrow), AC and AD (black arrows) for injection in area A, and BA (double headed grey arrow), BC and BD (orange arrows) for injection in area B. Consistency would imply, for example, that for a distance measure, d, the estimate of $d_{AB} = d_{BA}$ would be the same for both injections, i.e., $d_{CA} - d_{CB} = d_{DA} - d_{DB}$.

Figure 5. SLN Transformation. Comparison of logit (solid) and probit (dashed) transformations of SLN values on the interval (0, 1). The logit SLN is defined as ln(SLN/(1 – SLN)). The probit is defined as the inverse of the Gaussian cumulative distribution function and is often notated by Φ^{-1}. The scale factor of the logit curve has been adjusted by a factor of 0.588 to match it to the probit curve.

Figure 6. Probit transformation. Scatter plots of probit transformed SLN values of common source areas from pairs of 11 visual areas, obtained from retrograde tracer injections. The absicssa of each graph corresponds to the transformed SLN values of area *i*, indicated on the diagonal at the top of the column and the ordinate values are the transformed SLN values of area *j* indicated on the diagonal at the right of the row. The dashed blue line in each plot is the best fit line of unit slope (replotted from (Markov et al., 2014b)).

Figure 7. Logit transformation. Scatter plots of logit transformed SLN values of common source areas from pairs of 8 somatosensory and motor areas, obtained from retrograde tracer injections. The plots follow the same format as in Figure 6 except that the SLN values from each axis are transformed by the logit function. The dashed blue line in each plot is the best fit line of unit slope.

Figure 8 Hierarchical organization of visual areas (left) estimated from the beta-binomial model. The model only provides the vertical level of the areas with respect to the lowest level. For clarity of presentation, we have separated them laterally into ventral and dorsal stream areas. The estimated values are only unique up to adding a constant and multiplying by a coefficient. Here, we have the areas to span the range 1-10. The right scatter plot shows the empirical SLN values plotted against those predicted by the model. The solid line is the unit slope line through the origin and the dashed line is the best fit linear regression.

Figure 9. Hierarchical distance. The hierarchical distance, h_{ij}, between common projections from areas *i* and *j* to area p, defined as the difference of logits of their SLN values, is equivalent to the log of the ratio of their supra- to infra-granular projection strengths to area *p*. a. This definition implies that the ratio between the laminar ratios of areas *i* and *j* to area *p* (orange arrows) is the same as that for any other target area *q* receiving projections from the same source areas (blue arrows), as formalized in the equation below the diagram. This is because the hierarchical distance from *i* to *j* should be the same for injections in both areas *p* and *q*. b. A rearrangement of the equation (below) implies, also, that the ratio between the laminar ratios of projections from a common soure area, *i*, to areas *p* and *q*, will be the same for any other common source area, *j*, to the same target areas.

Figure 10. Cortical-cortical strong loops. The strength-distance relation of 1615 projections from 91 to 29 cortical areas obtained from retrograde tracer injections. The transparent black points indicate all of the projections except those that participate in strong-loops in beige. The color gradient on these symbols corresponds to SLN strength as indicated by the inset color bar. The black line is the best fit linear regression to the transparent black points and the blue line is the best fit to the strong-loops. The F-statistic indicates the result of a nested likelihood test indicating the probability of a difference in strength between the two sets of points as large as that obtained under the null hypothesis that the true difference is zero, when physical distance via the WM is taken into account.

Figure 11. Left. Scatter plots of logit transformed SLN values of common source areas from pairs of 9 frontal and pre-frontal areas, obtained from retrograde tracer injections. The plots follow the same format as previous in Figures 6 and 7. The dashed blue line in each plot is the best fit line of unit slope. Right. Hierarchical scale values estimated for the 9 areas based on the proposed statistical model. Area F1 was assigned a value of 0 for model identifiability.

Figure 12 Dual counterstream architecture of inter-areal pathways. a. Parent neurons at L3 and L5 have FF projections (red) to higher order areas reciprocated by FB projections (blue) in L2 and the L6. Simultaneous tracer injections in high and low areas show that the upper layer counterstream has near 100% segregation, i.e. the FF (FB) neurons do not send axon collaterals to lower (higher) order areas. However the evidence that the FF and FB pathways form continuous streams, as depicted here is indirect; what crucially remains to be elucidated are the laminar details on the connectivity and the cellular targets. b. the canonical microcircuit showing the two FB pathways targeting L2 and L6. Modified from (Douglas and Martin, 1991); c. the incorrectly assumed serial processing (lower) between areas that is not observed in the cortex, where instead each areas project to all upper and lower stream areas (all to all). (panel a from (Markov et al., 2014b));

Figure 13 Distance effects of labeling in individual layers. This figure shows how differential changes in labeling in individual sublayers leads to the characteristic SLN found in up- and down stream areas to a cortical injection. Hence the short-distance spread of labeled neurons in L2 coupled with the long-distance spread in L6 leads to the observed decrease in SLN with increasing FB hierarchical distances. Likewise the long-distance spread of labeled neurons in L3 coupled with the short-distance spread in L5 leads to the observed increase in SLN with increasing FF hierarchical distances.

Figure 14. Schematic circuit for the interplay between bottom-up and top-down signaling characterized by differential frequency-band synchrony. In a reciprocally connected loop between a sensory-type area and a cognitive-type area, neural circuits in the superficial layers are endowed with strong intrinsic synaptic connections and generate stochastic oscillations in the gamma frequency range, whereas the deep layers have a propensity to display slower oscillations in the lower beta or alpha frequency range. Top-down projections originate in the deep layers and innervate pyramidal cells (brown), as well as dendrite-targeting (purple) and perisoma-targeting (blue) inhibitory interneurons. In this scenario, low beta/alpha oscillations are directly involved in top-down signaling, which interacts with locally generated gamma oscillations. Adopted with permission from Wang (Wang, 2010).

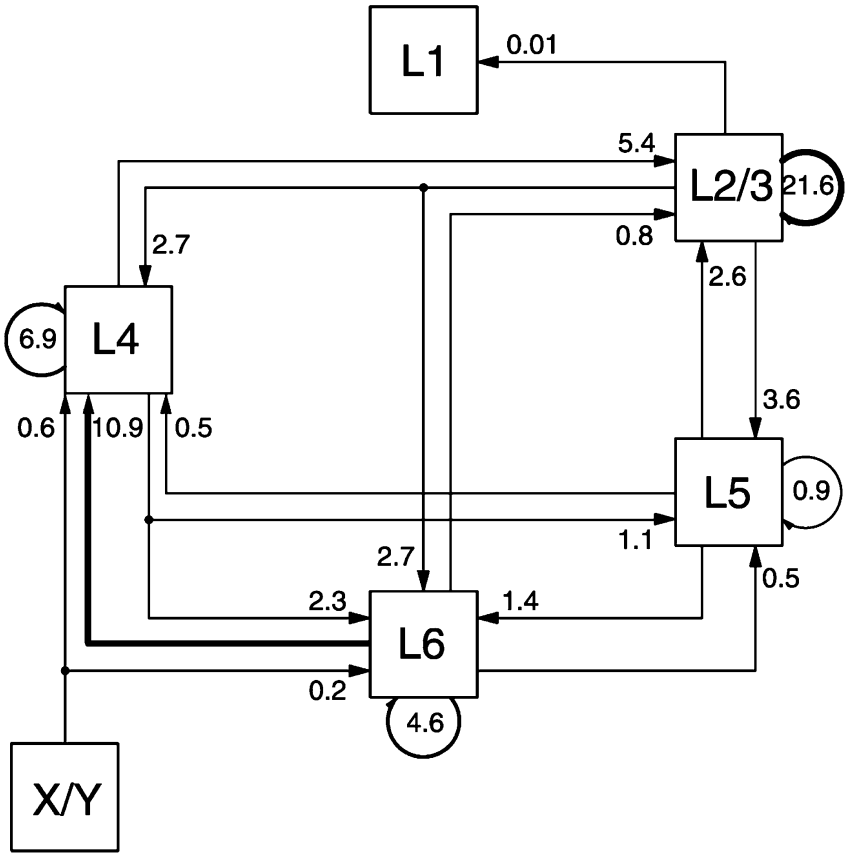

Figure 1. Quantitative map of excitatory synapses between excitatory neurons of the local microcircuit in visual cortex (area 17) of the cat. The feedforward loop starts in layer 4, the major thalamic recipient layer and then extends to layers 2/3, 5 and 6 with recurrent inputs back to layer 4. This feedforward loop corresponds to a little less than half of synapses involved in self-innervation of individual cortical layers. X/Y refers to the component cells of the lateral geniculate nucleus, the major thalamic relay. The original canonical microcircuit is shown in figure 12b. L refers to layer. From (Binzegger et al., 2004) with permission.

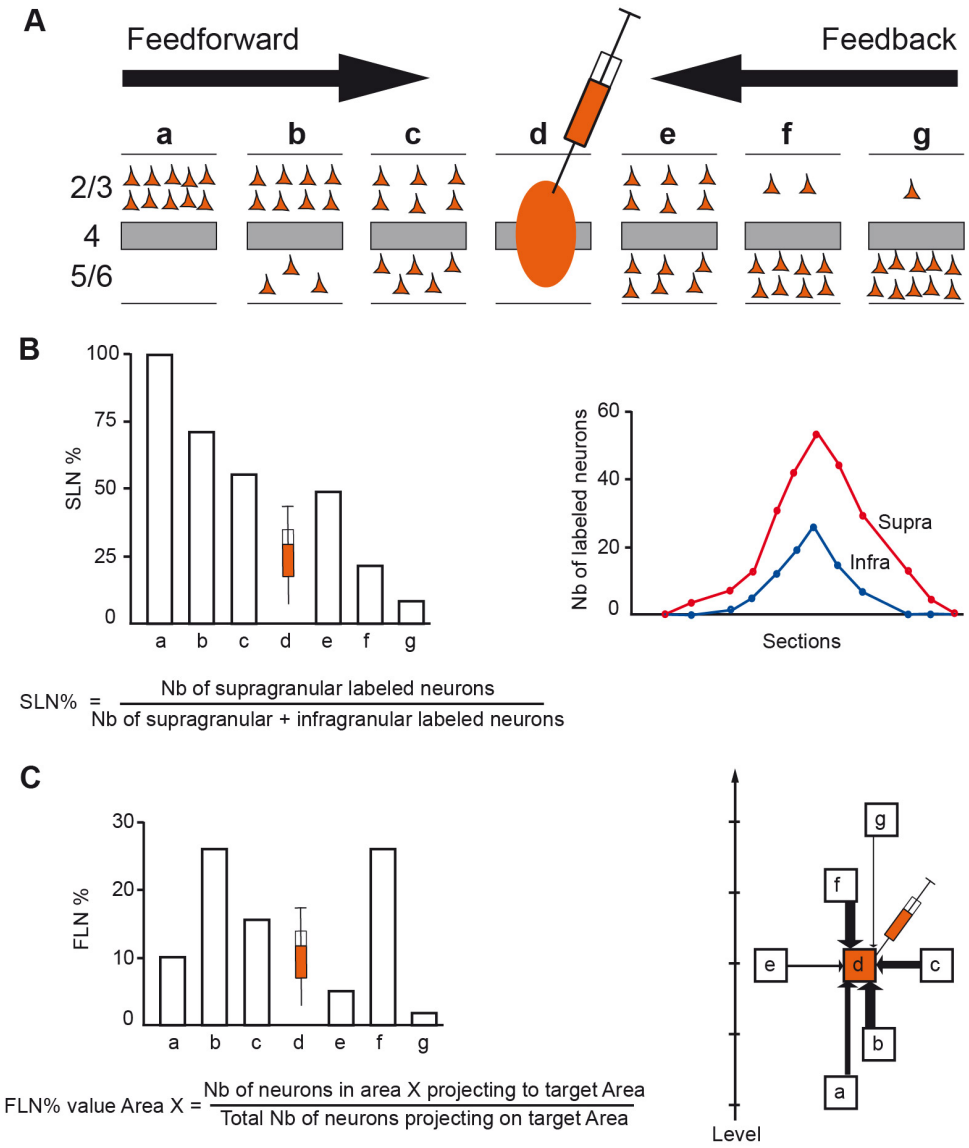

Figure 2. Quantitative parameters characterizing the hierarchy. A: The laminar distribution of parent neurons in each pathway, referred to as SLN (fraction of supragranular neurons) is determined by high frequency sampling and quantitative analysis of labeling. Supra- and infragranular layer neurons contribute to both feedback and feedforward pathways, and their relative proportion is characteristic for each type of pathway. For a given injection there is a gradient of SLN of the labeled areas, between purely FF (SLN = 100%, all the parent neurons are in the supragranular layers) to purely FB (SLN = 0%, all the parent neurons in the infragranular layers) and a spectrum of intermediate proportions; **B**: All labeled areas can then be ordered by decreasing SLN values and this order is consistent with hierarchical order according to Felleman and Van Essen. SLN is thus used as an indicator of hierarchical distance between areas from the same injection (Barone et al., 2000; Vezoli et al., 2004); **C**: FLN (fraction of labeled neurons) indicates the relative strength of each pathway (in number of labeled neurons) compared to the total number of neurons that are labeled in the cortical hemisphere after the injection. It requires counting labeled neurons from sections spanning the whole brain, but gives insight into the weight of connections. Vezoli et al. (Vezoli et al., 2004) showed that short-distance connections have high FLN values, whereas the strength of connection decreases as physical distance between source and target areas increases.

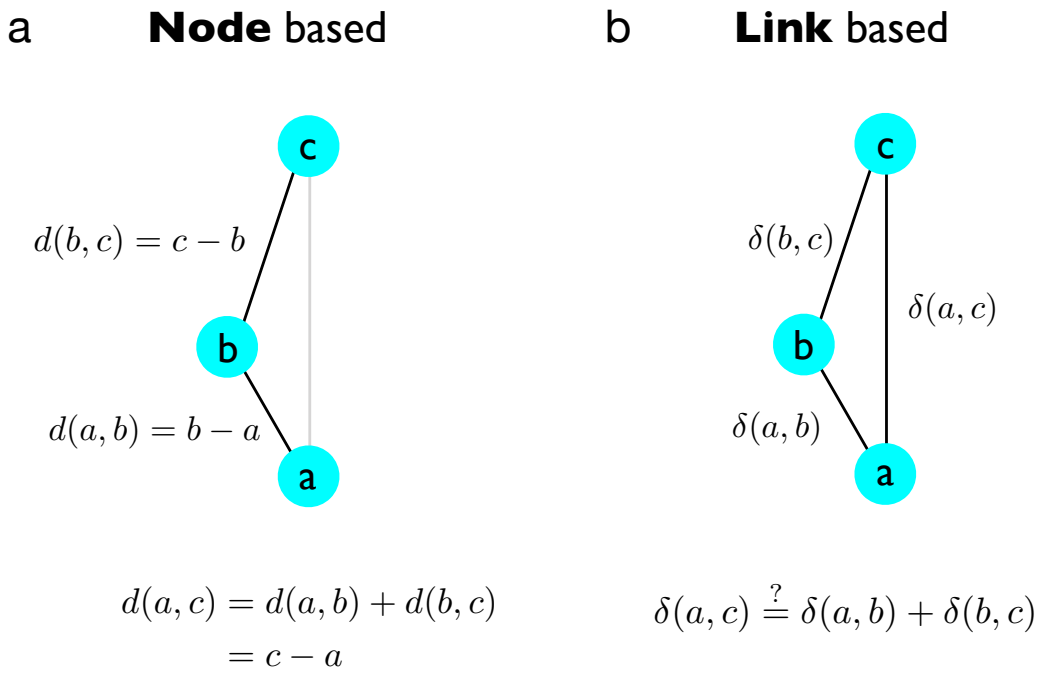

Figure 3. Properties of nodes and links. Nodes have fixed properties, a, b, c which in turn fixes their order and any distance measure, d, calculated from these properties. b. Link properties depend on the relations between node pairs, ab, bc, ac. The distance measures, δ, for ab, and bc do not necessarily fix that for ac. The above graphs are unidirectional, but in bi-directional graphs the distances between nodes need not by symmetric.

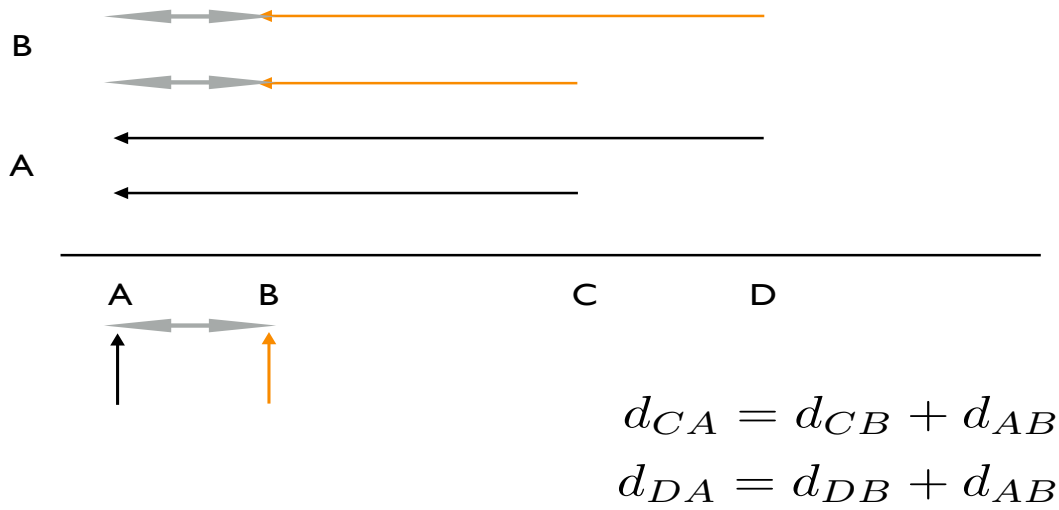

Figure 4. Hierarchical scales. Suppose a hierarchical scale between areas A, B, C, D, with the ordering and distances as illustrated on the bottom line. We expect measures of distance to be consistent measured between any pairs of areas. For example, injections in areas A and B lead to distances defined with respect to each of these areas, i.e., distances AB (double headed grey arrow), AC and AD (black arrows) for injection in area A, and BA (double headed grey arrow), BC and BD (orange arrows) for injection in area B. Consistency would imply, for example, that for a distance measure, d, the estimate of $d_{AB} = d_{BA}$ would be the same for both injections, i.e., $d_{CA} - d_{CB} = d_{DA} - d_{DB}$.

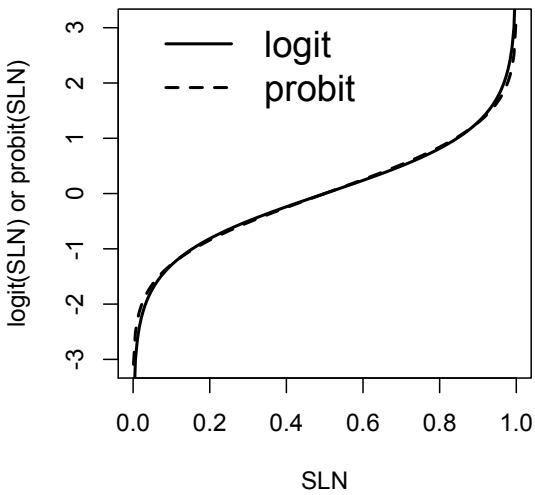

Figure 5. SLN Transformation. Comparison of logit (solid) and probit (dashed) transformations of SLN values on the interval (0, 1). The logit SLN is defined as ln(SLN/(1 – SLN)). The probit is defined as the inverse of the Gaussian cumulative distribution function and is often notated by Φ^{-1}. The scale factor of the logit curve has been adjusted by a factor of 0.588 to match it to the probit curve.

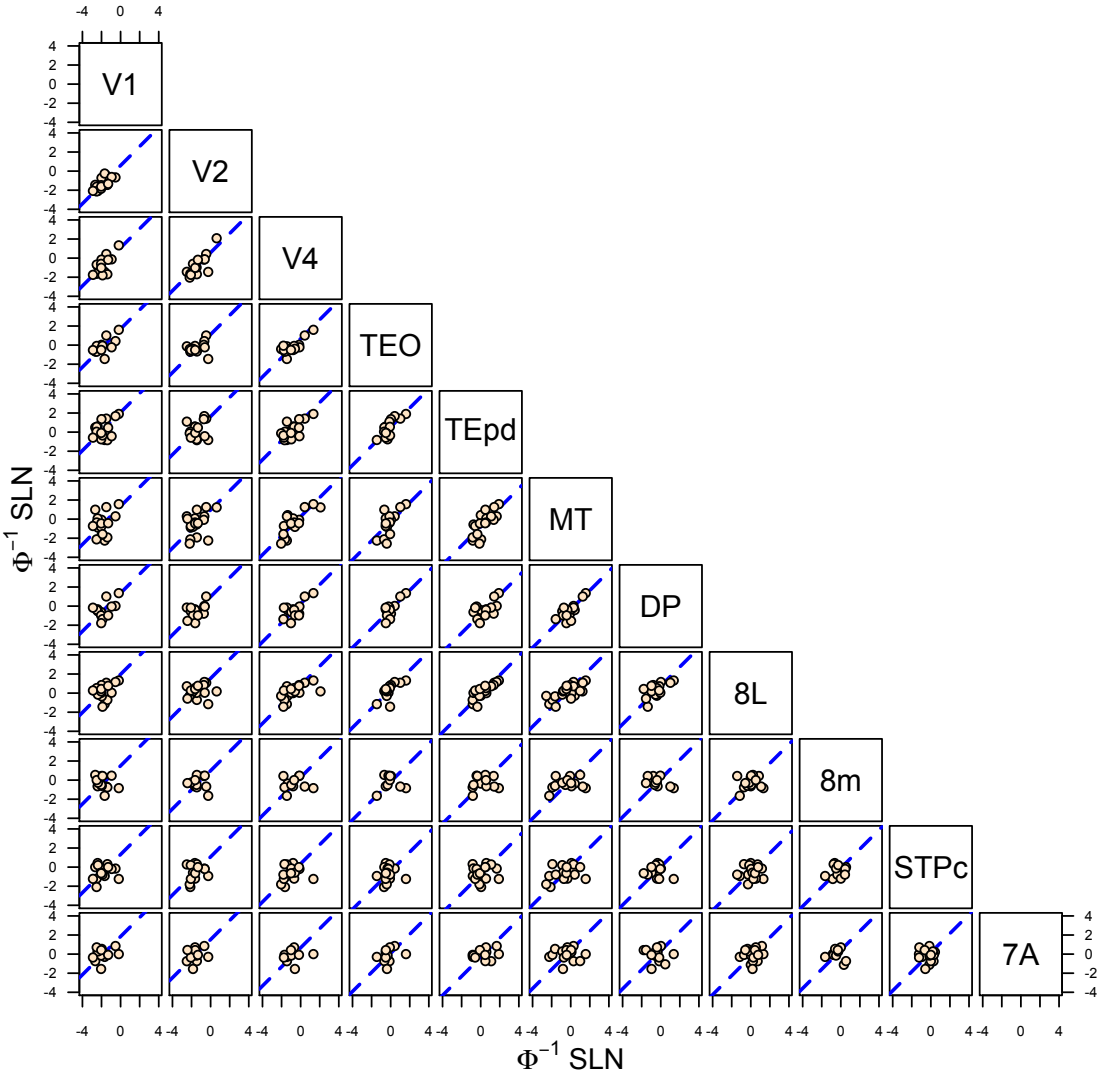

Figure 6. Probit transformation. Scatter plots of probit transformed SLN values of common source areas from pairs of 11 visual areas, obtained from retrograde tracer injections. The absicssa of each graph corresponds to the transformed SLN values of area *i*, indicated on the diagonal at the top of the column and the ordinate values are the transformed SLN values of area *j* indicated on the diagonal at the right of the row. The dashed blue line in each plot is the best fit line of unit slope (replotted from (Markov et al., 2014b)).

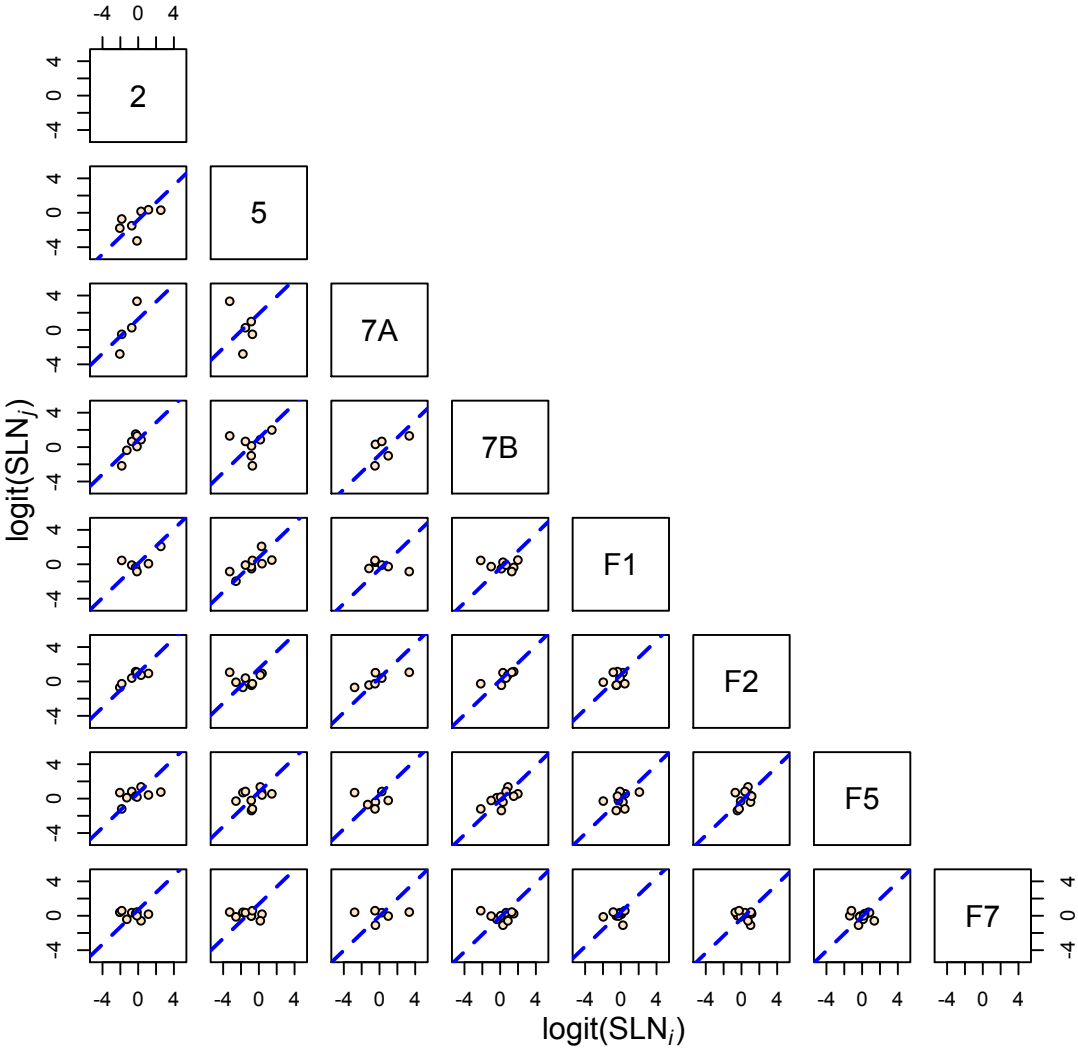

Figure 7. Logit transformation. Scatter plots of logit transformed SLN values of common source areas from pairs of 8 somatosensory and motor areas, obtained from retrograde tracer injections. The plots follow the same format as in Figure 6 except that the SLN values from each axis are transformed by the logit function. The dashed blue line in each plot is the best fit line of unit slope.

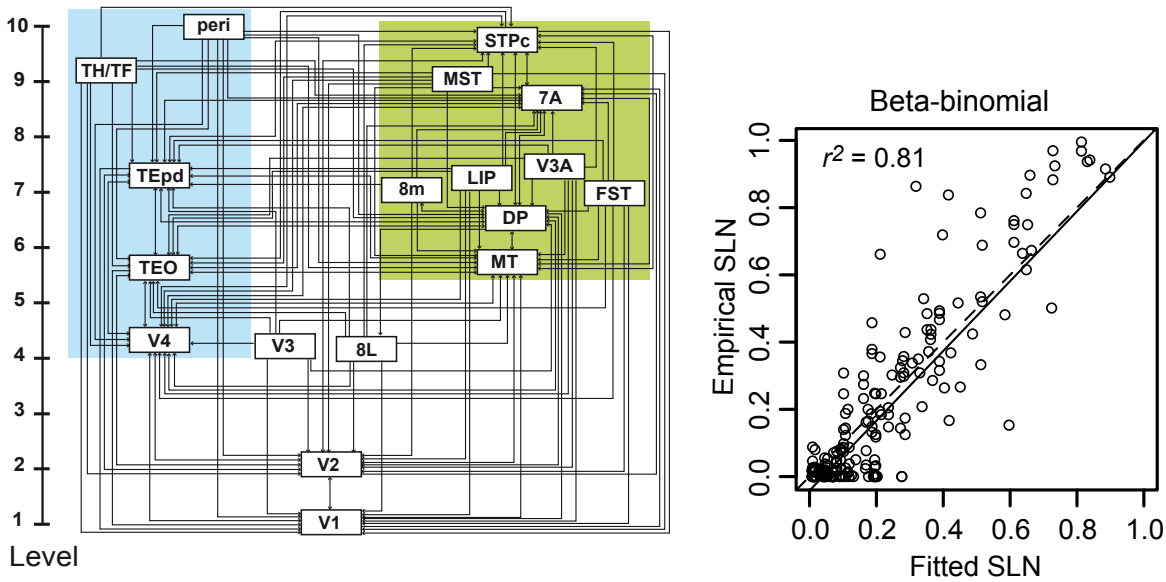

Figure 8 Hierarchical organization of visual areas (left) estimated from the beta-binomial model. The model only provides the vertical level of the areas with respect to the lowest level. For clarity of presentation, we have separated them laterally into ventral and dorsal stream areas. The estimated values are only unique up to adding a constant and multiplying by a coefficient. Here, we have the areas to span the range 1-10. The right scatter plot shows the empirical SLN values plotted against those predicted by the model. The solid line is the unit slope line through the origin and the dashed line is the best fit linear regression.

$$h_{ij} = \text{logit}(\text{SLN}_p^i) - \text{logit}(\text{SLN}_p^j) = \log S_p^i/I_p^i - \log S_p^j/I_p^j = \log\left(\frac{S_p^i/I_p^i}{S_p^j/I_p^j}\right)$$

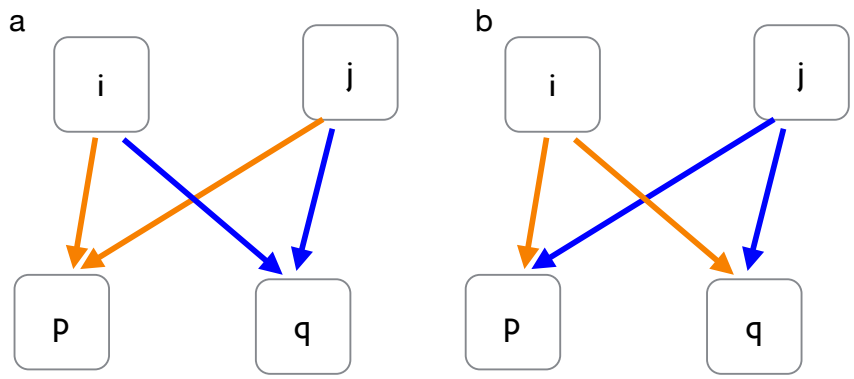

$$\frac{S_p^i/I_p^i}{S_p^j/I_p^j} = \frac{S_q^i/I_q^i}{S_q^j/I_q^j}, \qquad \frac{S_p^i/I_p^i}{S_q^i/I_q^i} = \frac{S_p^j/I_p^j}{S_q^j/I_q^j}.$$

Figure 9. Hierarchical distance. The hierarchical distance, h_{ij}, between common projections from areas *i* and *j* to area p, defined as the difference of logits of their SLN values, is equivalent to the log of the ratio of their supra- to infra-granular projection strengths to area *p*. a. This definition implies that the ratio between the laminar ratios of areas *i* and *j* to area *p* (orange arrows) is the same as that for any other target area *q* receiving projections from the same source areas (blue arrows), as formalized in the equation below the diagram. This is because the hierarchical distance from *i* to *j* should be the same for injections in both areas *p* and *q*. b. A rearrangement of the equation (below) implies, also, that the ratio between the laminar ratios of projections from a common soure area, *i*, to areas *p* and *q*, will be the same for any other common source area, *j*, to the same target areas.

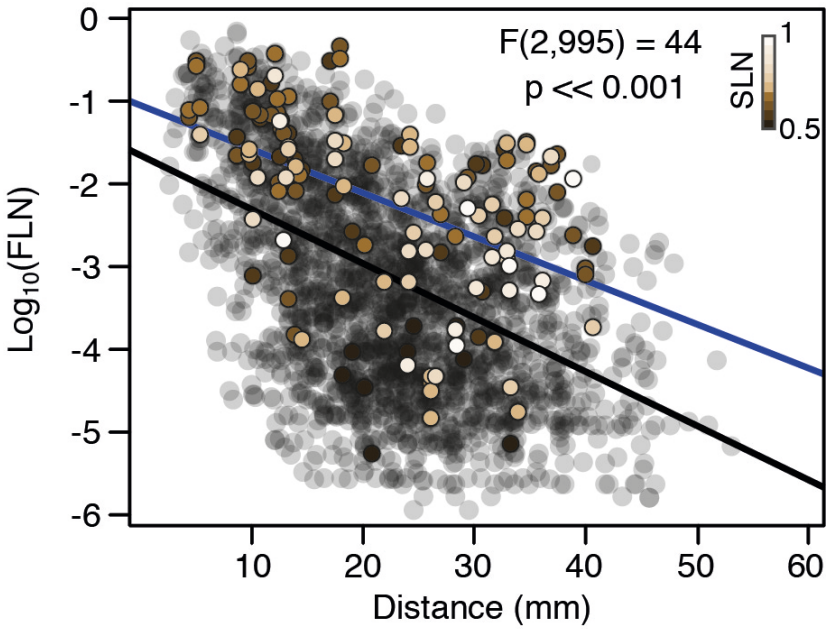

Figure 10. Cortical-cortical strong loops. The strength-distance relation of 1615 projections from 91 to 29 cortical areas obtained from retrograde tracer injections. The transparent black points indicate all of the projections except those that participate in strong-loops in beige. The color gradient on these symbols corresponds to SLN strength as indicated by the inset color bar. The black line is the best fit linear regression to the transparent black points and the blue line is the best fit to the strong-loops. The F-statistic indicates the result of a nested likelihood test indicating the probability of a difference in strength between the two sets of points as large as that obtained under the null hypothesis that the true difference is zero, when physical distance via the WM is taken into account.

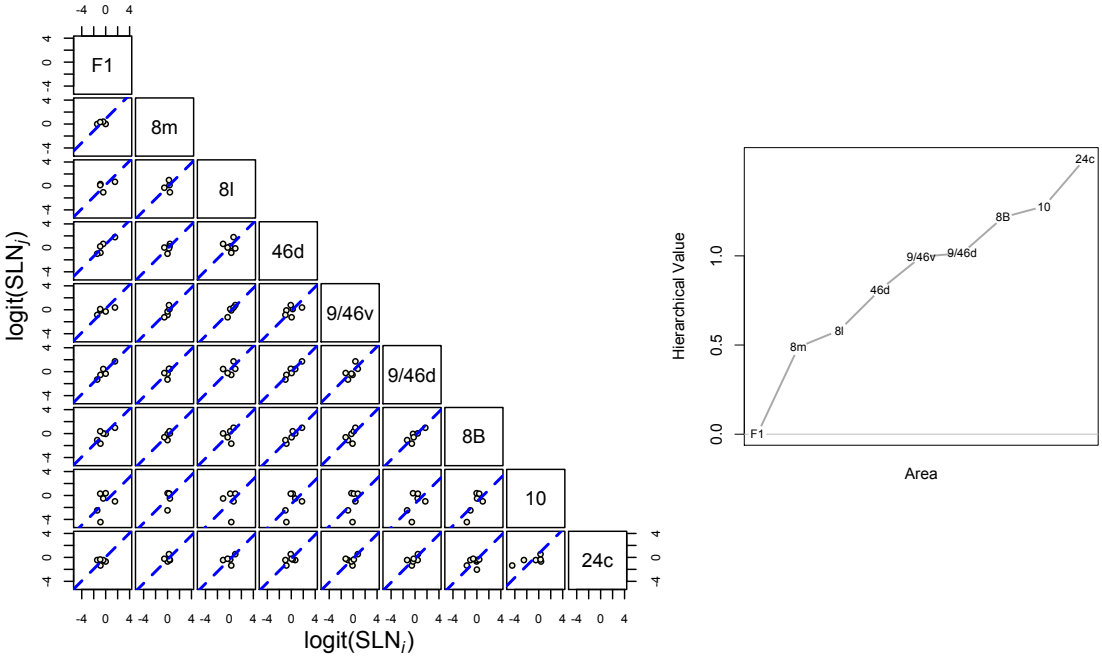

Figure 11. Left. Scatter plots of logit transformed SLN values of common source areas from pairs of 9 frontal and pre-frontal areas, obtained from retrograde tracer injections. The plots follow the same format as previous in Figures 6 and 7. The dashed blue line in each plot is the best fit line of unit slope. Right. Hierarchical scale values estimated for the 9 areas based on the proposed statistical model. Area F1 was assigned a value of 0 for model identifiability.

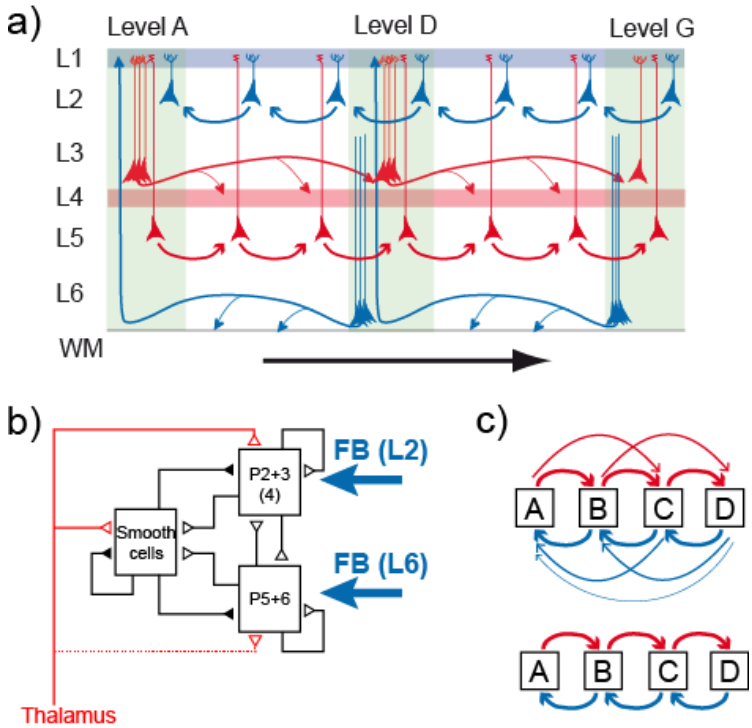

Figure 12 Dual counterstream architecture of inter-areal pathways. a. Parent neurons at L3 and L5 have FF projections (red) to higher order areas reciprocated by FB projections (blue) in L2 and the L6. Simultaneous tracer injections in high and low areas show that the upper layer counterstream has near 100% segregation, i.e. the FF (FB) neurons do not send axon collaterals to lower (higher) order areas. However the evidence that the FF and FB pathways form continuous streams, as depicted here is indirect; what crucially remains to be elucidated are the laminar details on the connectivity and the cellular targets. b. the canonical microcircuit showing the two FB pathways targeting L2 and L6. Modified from (Douglas and Martin, 1991); c. the incorrectly assumed serial processing (lower) between areas that is not observed in the cortex, where instead each areas project to all upper and lower stream areas (all to all). (panel a from (Markov et al., 2014b));

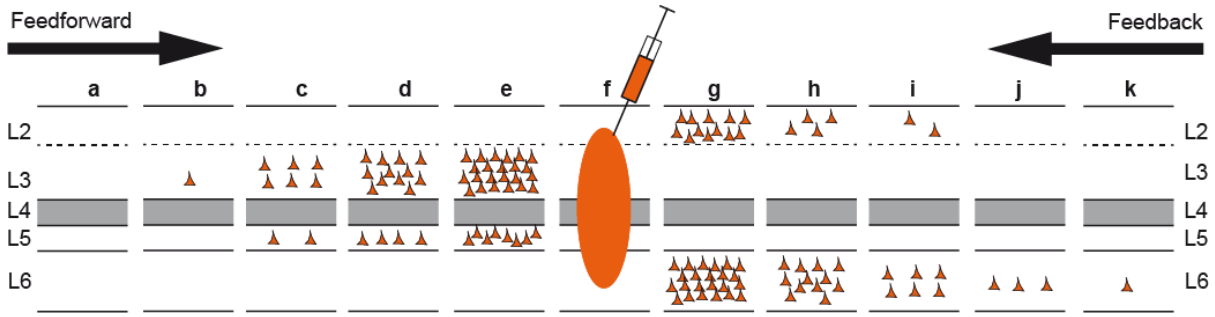

Figure 13 Distance effects of labeling in individual layers. This figure shows how differential changes in labeling in individual sublayers leads to the characteristic SLN found in up- and down stream areas to a cortical injection. Hence the short-distance spread of labeled neurons in L2 coupled with the long-distance spread in L6 leads to the observed decrease in SLN with increasing FB hierarchical distances. Likewise the long-distance spread of labeled neurons in L3 coupled with the short-distance spread in L5 leads to the observed increase in SLN with increasing FF hierarchical distances.

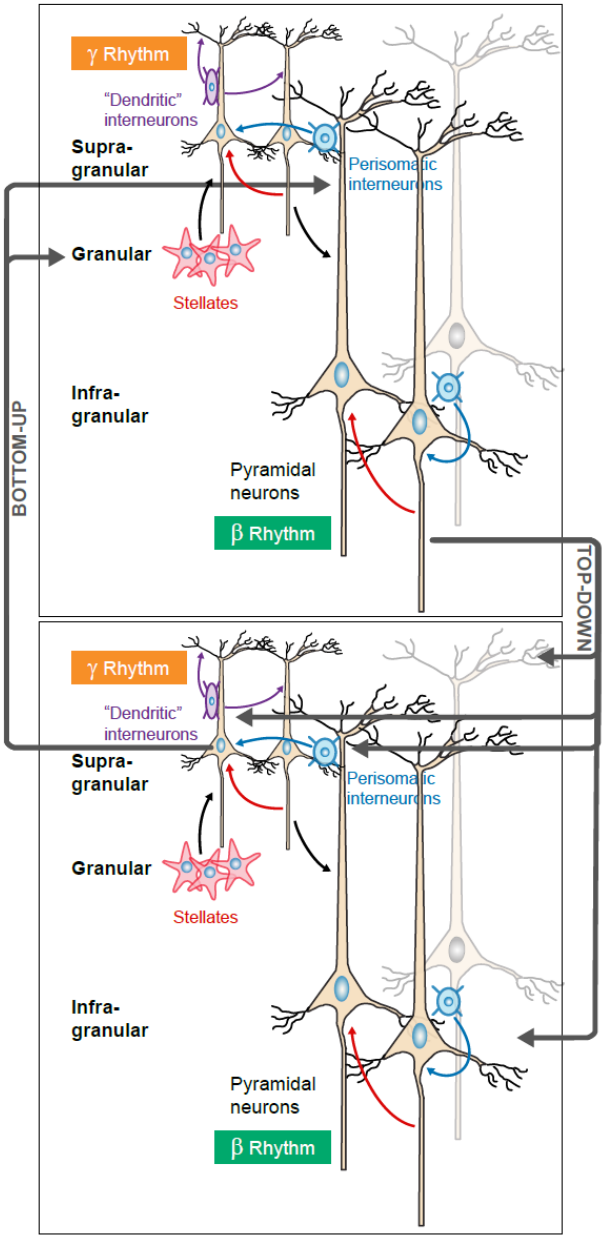

Figure 14. Schematic circuit for the interplay between bottom-up and top-down signaling characterized by differential frequency-band synchrony. In a reciprocally connected loop between a sensory-type area and a cognitive-type area, neural circuits in the superficial layers are endowed with strong intrinsic synaptic connections and generate stochastic oscillations in the gamma frequency range, whereas the deep layers have a propensity to display slower oscillations in the lower beta or alpha frequency range. Top-down projections originate in the deep layers and innervate pyramidal cells (brown), as well as dendrite-targeting (purple) and perisoma-targeting (blue) inhibitory interneurons. In this scenario, low beta/alpha oscillations are directly involved in top-down signaling, which interacts with locally generated gamma oscillations. Adopted with permission from Wang (Wang, 2010).